Natural Resources Canada | Ressources naturelles Canada

GEOLOGICAL SURVEY OF CANADA
OPEN FILE 8100

Preliminary Results of a Magnetotelluric Survey Across the Brock Inlier, Northwest Territories

J.E. Spratt, J.A. Craven, and R.H. Rainbird

2016

Canada

GEOLOGICAL SURVEY OF CANADA
OPEN FILE 8100

Preliminary Results of a Magnetotelluric Survey Across the Brock Inlier, Northwest Territories

J.E. Spratt[1], J.A Craven[2] and R.H. Rainbird[2]

[1] Magnetotelluric Contractor, Wakefield, Quebec J0X 3G0
[2] Geological Survey of Canada, 601 Booth St., Ottawa, ON K1A 0E8

2016

doi:10.4095/299099

This publication is available for free download through GEOSCAN (http://geoscan.nrcan.gc.ca/).

Recommended citation
Spratt, J.E., Craven, J.A., and Rainbird, R.H., 2016. Preliminary results of a magnetotelluric survey across the Brock Inlier, Northwest Territories; Geological Survey of Canada, Open File 8100, 41 p. doi:10.4095/299099

Publications in this series have not been edited; they are released as submitted by the author.

This report is dedicated to the memory of Frances Wolki

1.0 Introduction

The Brock Inlier Project, Northwest Territories, is part of the second phase of Natural Resources Canada's Geo-mapping for Energy and Minerals (GEM) program. It involves stratigraphic analysis and geological mapping of uplifted mostly late Mesoproterozoic to early Neoproterozoic sedimentary units and surrounding Paleozoic and Mesozoic sedimentary rocks (Rainbird et al., 2015a,b). The Brock Inlier overlaps the eastern edge of the largest gravity and magnetic anomaly in North America, the Darnley Bay anomaly. It has been suggested that the anomaly is a result of a deeply buried Ni-Cu-PGE magmatic sulphide deposit similar to that of Noril'sk in Russia (Jones et al., 1992, Jefferson et al., 1994). Magnetotelluric (MT) data have been acquired along an east-west transect to trace sedimentary rocks layers westward from the Brock Inlier into the subsurface and to improve our understanding of the nature, size and depth of the Darnley Bay anomaly.

Co-located audio- (AMT) and broadband (BBMT) magnetotelluric sites were collected at 17 locations during the 2015 summer field (Figure 1a). The transect crosses Mesozoic rocks along the southern margin of the Darnley Bay anomaly then crosses over onto Proterozoic rocks of the Brock Inlier along the eastern margin of the anomaly . The Darnley Bay MT data have been processed using modern, robust methods and have been analyzed for non-uniform source fields, dimensionality, effects of distortion, geo-electric strike angles and ocean sea water effects. Electrical resistivity profiles derived from rigorous 2D inversions of the MT impedance tensor highlight areas of low resistivity. These low resistivities are commonly associated with rock types containing conductive mineral assemblages or may represent a proxy for zones of deformation, fault zones, and fossil fluid pathways. Here we present and discuss two-dimensional resistivity models along the MT transect.

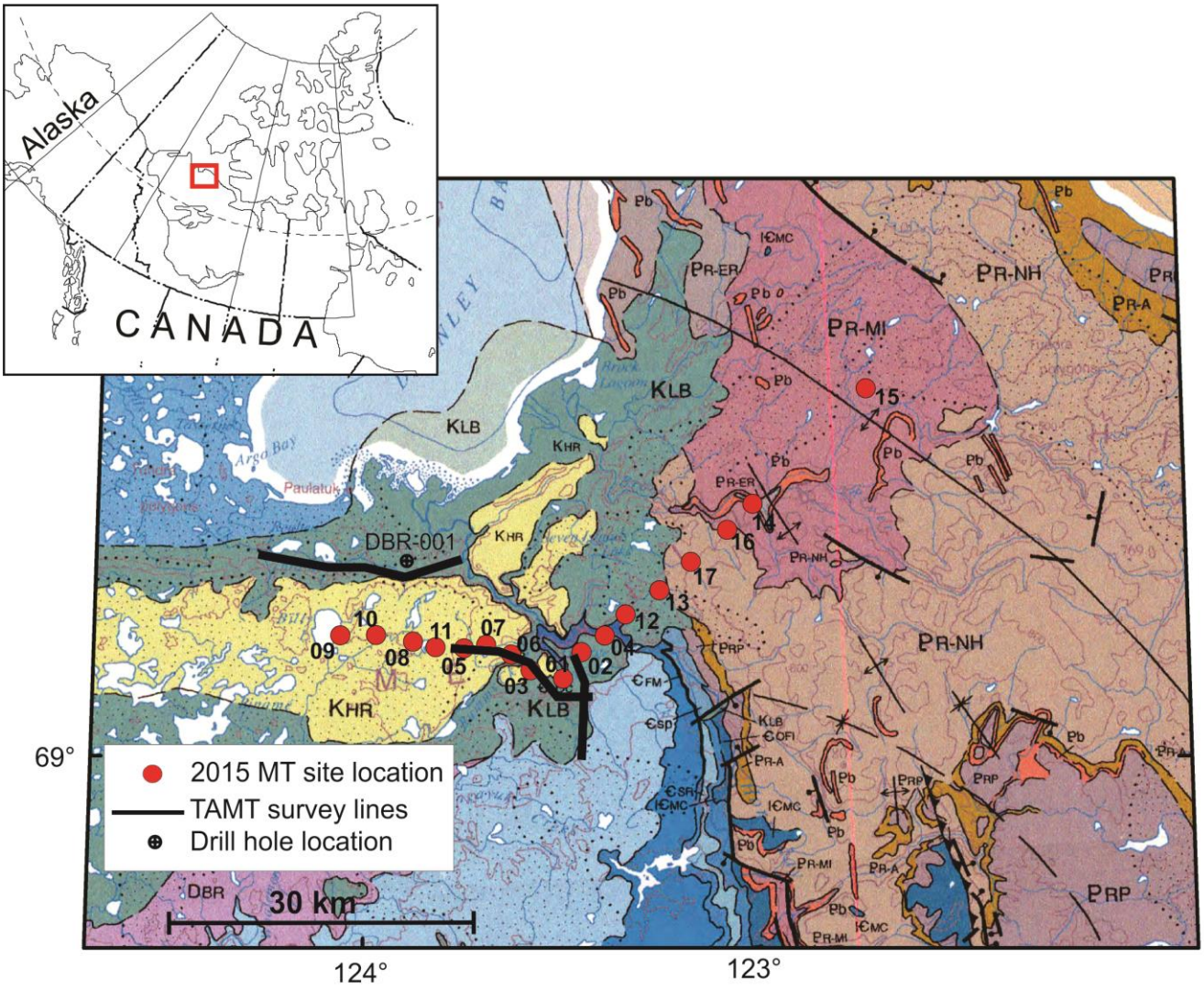

Figure 1 Locations of MT stations (red circles) overlain on regional geological map of the Brock Inlier. Modified from Okulitch (2000). K, D, S, O, Є, P = Cretaceous, Devonian, Silurian, Ordovician, Cambrian, and Proterozoic units respectively.

2.0 Geological and Geophysical Background

The Brock Inlier and Darnley Bay region is largely obscured by up to 1 km of Phanerozoic sediments that consist primarily of unconsolidated Pleistocene glacial sediments overlying mostly silicified carbonates of the Cambrian Ronning Group and/or the Franklin Mountain Formation (Jones et al., 1992). These are underlain by the early Neoproterozoic Reynolds Point and Rae groups of the Shaler Supergroup, including sandstone, mudrock and dolostone that are up to 1.5 km thick (Figure 1)(Rainbird et al., 1994; Rainbird et al.,1996; Reford, 2012). The Shaler Supergroup is intruded by 718-723 Ma mafic dykes and sills of the Franklin large igneous province (Heaman et al., 1992). Below the Shaler Supergroup lies flood basalt and sandstone of the Coppermine River Group (Baragar and Donaldson, 1973), carbonates of the Dismal Lakes Group and sandstones of the Hornby Bay Group estimated to be 3-4km in thickness (MacLean and Cook, 1992; Cook and MacLean 2004). Aspler et at.

(2003) show that the basement beneath the Brock Inlier and Darnley Bay anomaly is part of the Slave craton, but recent work by Schaeffer and Lebedev (2014) place it within the Mackenzie craton.

Just west of the exposed Brock Inlier lies the Darnley Bay anomaly, a positive 130 mgal Bouguer gravity and coincident 750 nT positive magnetic anomaly (Figure 2 and Figure 3). It has been suggested (e.g. Jefferson et al., 1994) that the source of both the gravity and magnetic field anomalies is due to a large body of ultramafic to mafic rock that intrudes crystalline rocks of the Slave Province as well as some of the Proterozoic supracrustal rocks described above. Interpretation of the gravity and magnetic data show that the top of the intrusion lies at 1 – 5.5 km depth and extends as a truncated cone which widens with depth (Stacey, 1971). However, Jefferson et al. (1994) interpret the gravity data to represent steep sides to depths of 7 km. Seismic data acquired along the western margin of the Darnley Bay anomaly revealed east dipping reflectors that were first interpreted as the top of the intrusive body at depths of ~3048 – 3354 m, where an offset in the reflectors coincides with the western margin of the anomaly (Vye, 1972). The depth, size and internal structure of the Darnley Bay anomaly remains largely uncertain in that a unified model to explain all features remains elusive.

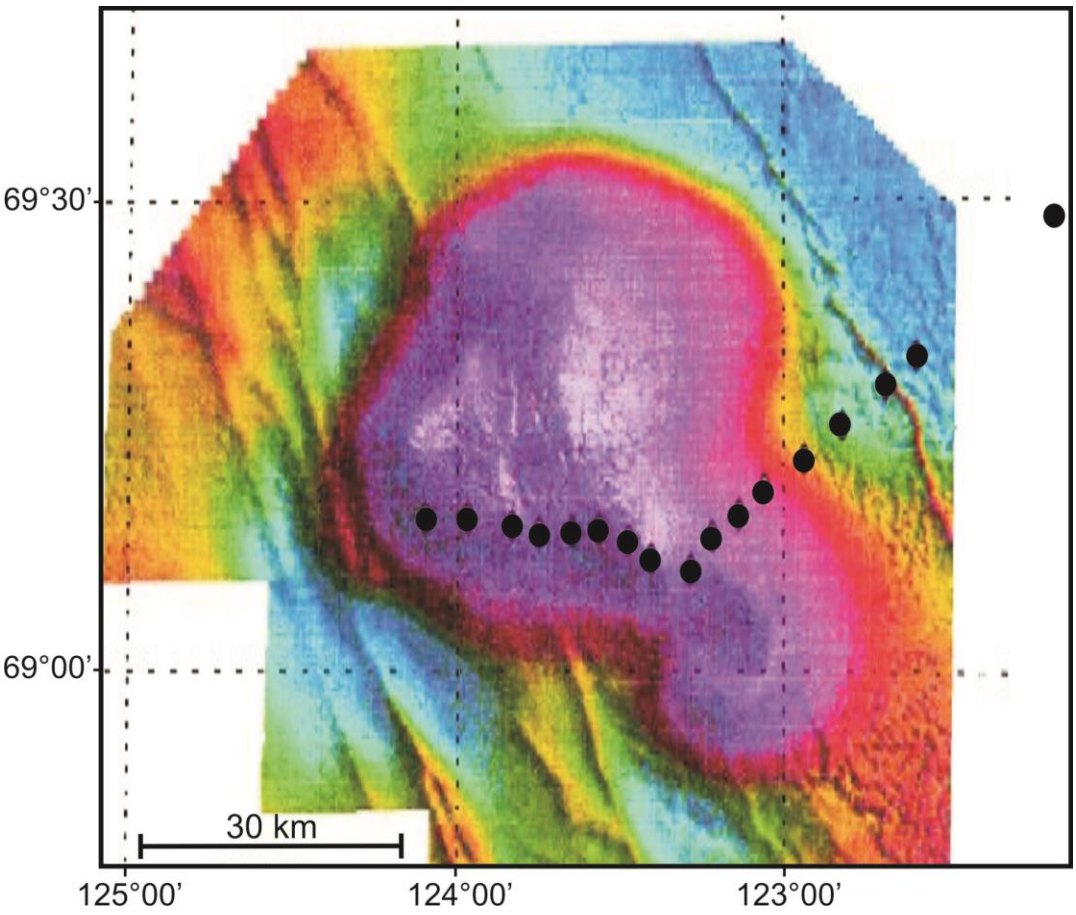

Figure 2 High resolution total magnetic field aeromagnetic map of Darnley Bay anomaly. The black circles represent the MT site locations. The northwestward trending linear features are interpreted as diabase Franklin dykes that postdate the main body. Modified after Cook and Maclean (2004).

A drill hole located within the Darnley Bay anomaly (Drill-hole DBR-001 on Figure 1a) reached a depth of 1812 m without intersecting the intrusive body (Reford, 2012). The core reveal Phanerozoic cover sediments to 377 m that overlie Cambrian sandstones to 1167 m. These are underlain by mudrocks interpreted to be representative of the Escape Rapids Formation the (early Neoproterozoic Shaler Supergroup, Rainbird et al., 1994, 2015b).

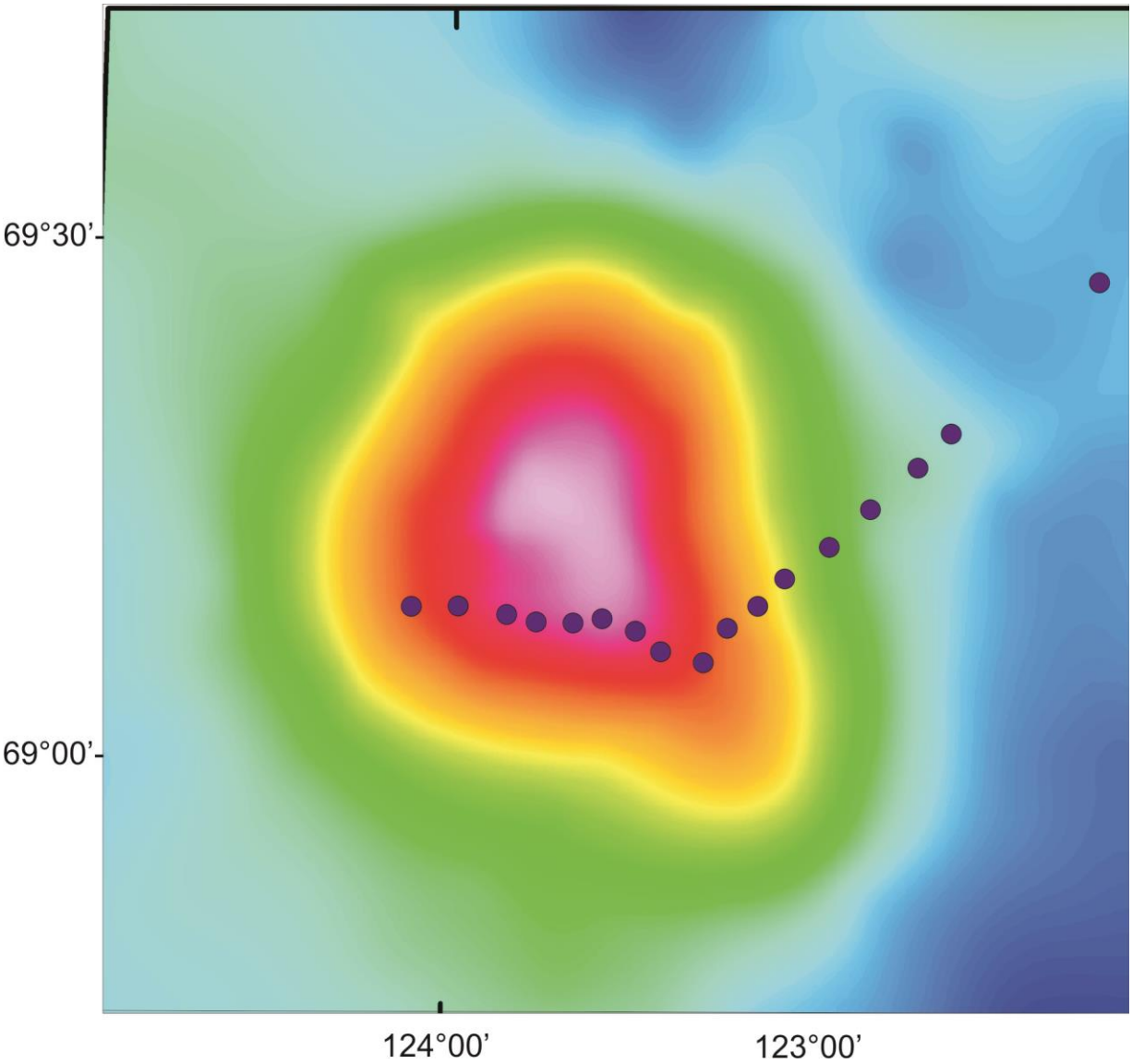

Figure 3 Map of the MT survey area showing the bouguer gravity data. Black circles shows MT site location.

Transient AMT data was collected at a 500 m station intervals by Empulse Geophysics LTD along three transects: (1) as east-west profile across the western margin of the anomaly, (2) and east-west profile across the eastern margin of the anomaly, and (2) a north-south profile east of the eastern margin of the anomaly (Figure 1; Goldak, 2014). The resistivity model along Profile 1 shows a near surface, moderately resistive layer (~500 ohm·m) that thickens from 50 m to ~200 m from west to east which is interpreted as Pleistocene glacial sediments (Goldak and Olsen, 2015). This is underlain by a

1 km thick resistive layer (>1000 ohm-m) that is suggested to result from the silicified carbonates of the Ronning Group and/or the Franklin Mountain formation. Beneath the resistive layer is a moderately conductive layer, with values of ~10 – 100 ohm·m, that coincides with the characteristics and thickness estimates of the Escape Rapids Formation. Resistivities then increase to ~700 ohm·m at 2.5 km depth in the west down to ~3 km in the east. This increase in resistivity is consistent with values estimated for both the intrusive body and the Dismal Lake Group, however the increase is coincident with east dipping seismic reflectors interpreted to represent the top of the intrusive body. Slightly decreased resistivities at these depths are observed near the western margin of the anomaly, where there is an offset in the seismic reflectors, and are interpreted as a bounding fault structure by Goldak and Olsen (2015).

3.0 Data Acquisition and processing

Audio magnetotelluric (AMT) and broadband (BBMT) data were collected at a total of 16 and 17 sites locations respectively using Phoenix Geophysics recording instruments and sensors along a ~90 km long NNE – SSW profile at a site spacing of roughly 5 km (Figure 1a). The electric fields were measured in the 2 horizontal perpendicular directions using lead-lead chloride porous pots, and the magnetic fields were recorded in the 2 horizontal and, where possible, the vertical directions. Generally 4 sites were acquired each day. Electric field data was recorded in the AMT and BBMT ranges at each site, with the exception of DBR06 where only BBMT data was acquired. For each day of recording, the horizontal AMT magnetic field data was recorded at one or two sites using Phoenix AMTC-30 coils and the BBMT magnetic field at another site using Phoenix MTC-50 coils. Where coils were not installed, the data were processed using the horizontal magnetic field components from neighboring sites (see Table 1). The vertical magnetic field data was acquired using Phoenix MTC-80 coils.

The time-series data were processed using robust remote-reference algorithms supplied by Phoenix Limited and based on the coherence-sorted cascade decimation method of Wight and Bostick (1981) and the heuristic robust approach of Jones and Jödicke (1984). Results yielded apparent resistivity and phase response curves in the period range of 0.0001 s up to 1,000 s for most sites along the profile (Figure 4). In general, the data quality is poor at periods below 0.001 s, particularly within the 0.0002 – 0.001 s AMT deadband (Figure 4a and b). The data quality is excellent at periods between 0.001 - 300 s, and up to 1000 s at some sites (Appendix A).

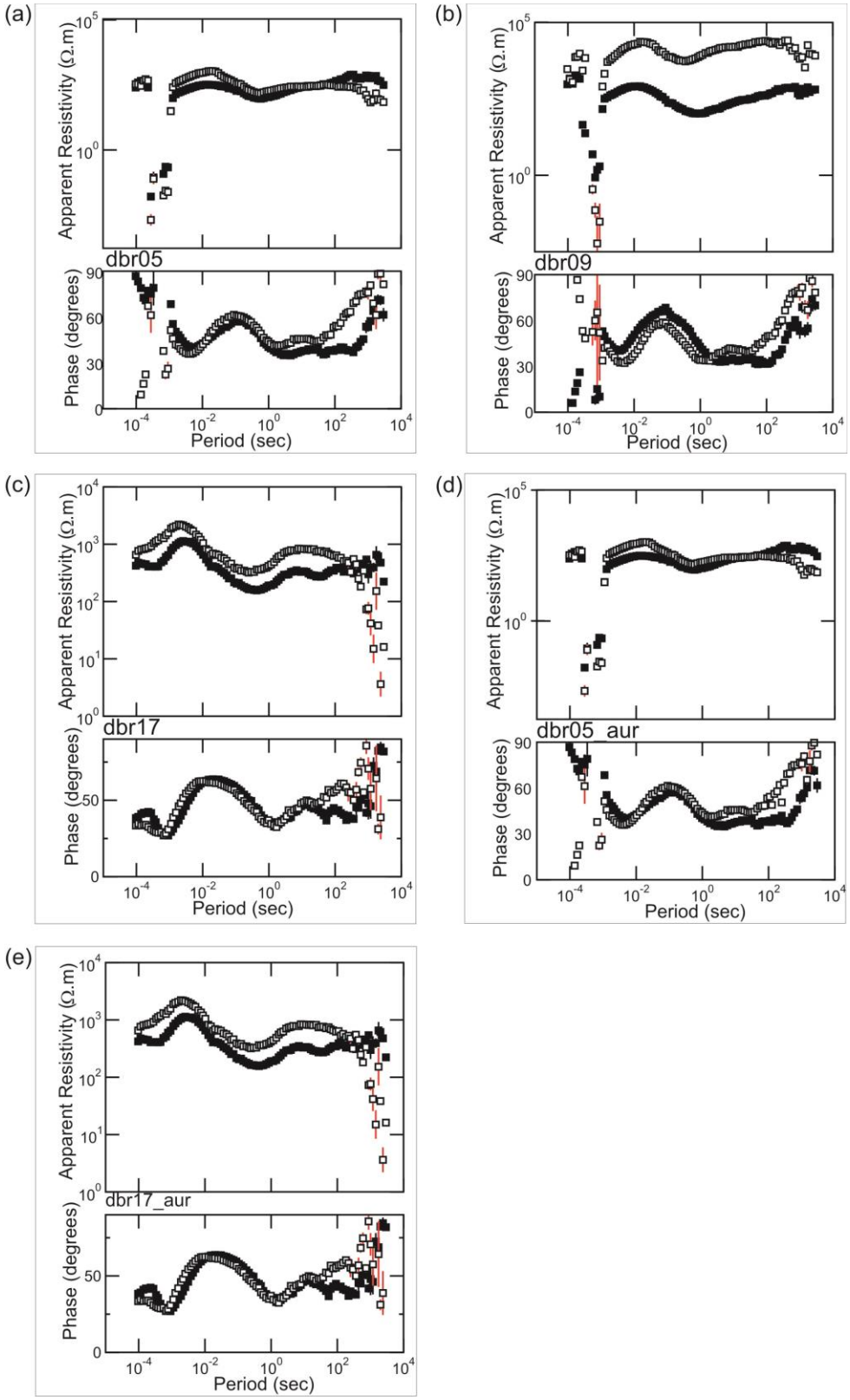

Figure 4 Example of MT soundings from three stations. The open squares show data measured in the north-south direction (XY response) and the closed squares show data measured in the east-west direction (the YX response). (a) shows an example of poor data quality at the long periods at site dbr05, (b) shows and example of anisotropy effects at site dbr09, (c) shows an example excellent quality at short periods within the AMT deadband at site dbr17, (d) shows site dbr05 with non-planar suspect data removed and (e) shows site dbr17 with non-planar suspect data removed.

4.0 Data analysis

4.1 Non-uniform source fields

Non-uniform source field effects, due to the auroral electrojet, often cause distortion on MT data collected at high latitudes (Mareschal, 1986). The distortion is typically seen as reduced apparent resistivity values, and increased phase values at long periods, and can cause the depth to asthenosphere to be underestimated by nearly 50 km (Jones and Spratt, 2002). Analysis of non-uniform source fields was applied by identifying odd hours of anomalously high source fields and removing cross-power estimates calculated from data acquired during these times, at periods greater than 120 s. The odd hours were determined based on anomalously high source fields recorded by Space Weather Canada near Cambridge Bay, Nunavut (see Appendix B). Two such suspect hours were identified during data acquisition and were defined by time segments where the hourly range of X and Z were > 200 and the maximum rate of change of X and Z were > 40. These hours occurred during the acquisition of sites dbr05, dbr07, dbr09 (hour 1), and dbr14, dbr15, dbr16, and dbr17 (hour 2). The response curves derived after removing the cross-powers calculated during these hours at periods greater than 120 s showed no significant difference at the long periods, indicating that non-uniform source field effects are negligible for these data (Figure 4d and e).

4.2 Strike and Dimensionality Analysis

Most MT modeling algorithms assume the area of interest to be geoelectrically 1-D or 2-D. A 3D, i.e. varying in 3 directions, electrical structure requires greater computational power to model the data and the earth models must be comparatively simple. In a 2-D modeling scenario, the direction of geoelectric strike is assumed to be consistent, i.e. there must not be any localized or off-profile geoelectrical property variations, and the strike direction must be known. Groom-Bailey decompositions, frequency dependent pseudosections, induction vectors and phase tensors have been analyzed to determine the dimensionality and geoelectric strike direction of the data. Sections of the data that are 1-D (independent of strike) are identified as well as sections that are influenced by 3-dimensionality and cannot be represented with a 2-D model.

Groom and Bailey (GB) decompositions provide a method to describe and separate the local parameters caused by galvanic distortions in the regional observed impedance tensor (Groom and

Bailey, 1989). This distortion modelling assumes that the regional structure is two-dimensional, but

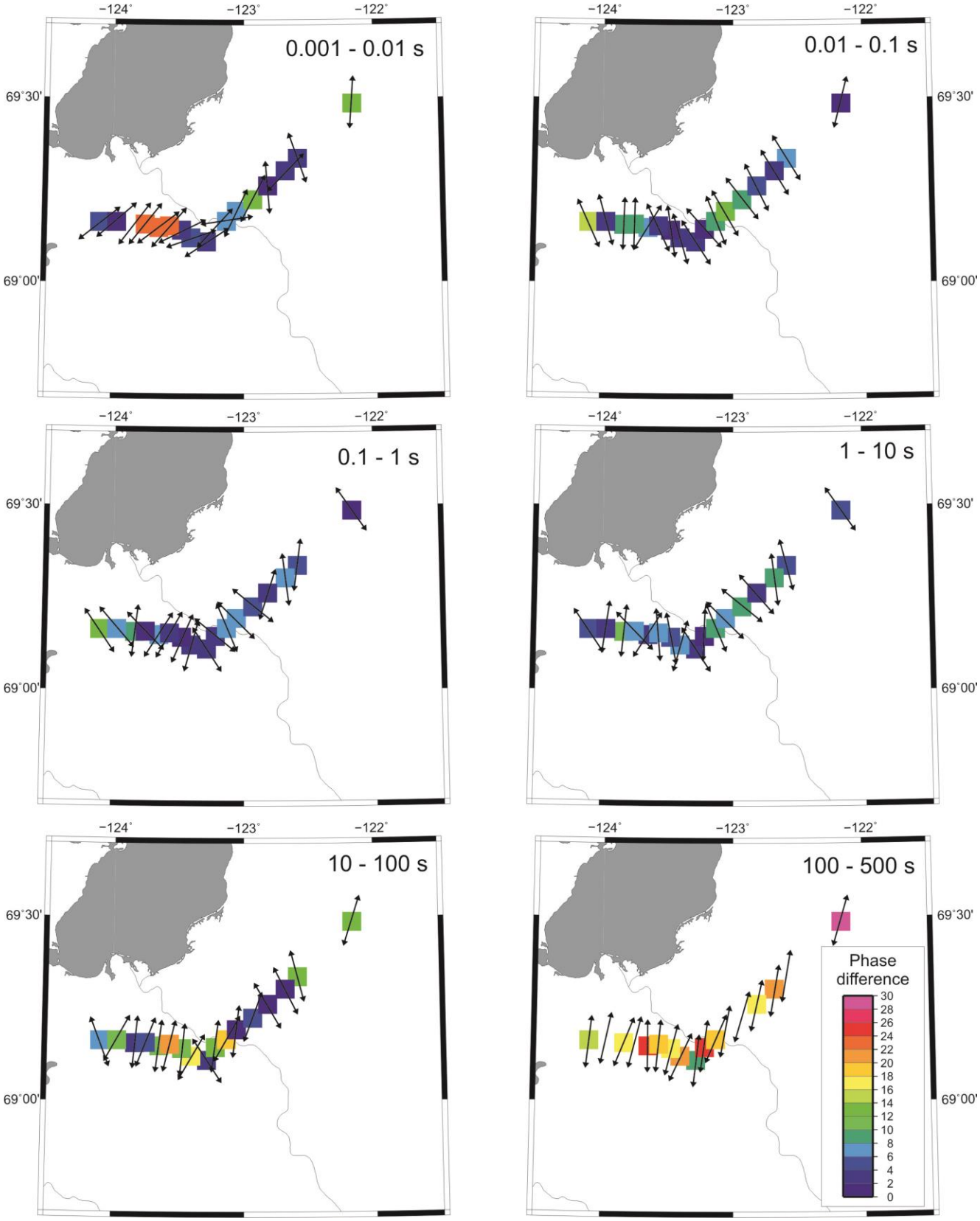

Figure 5 Maps showing the preferred geo-electric strike direction at each site for 6 decade period bands. The color scale illustrates the maximum difference between the TM- and TE-mode phases.

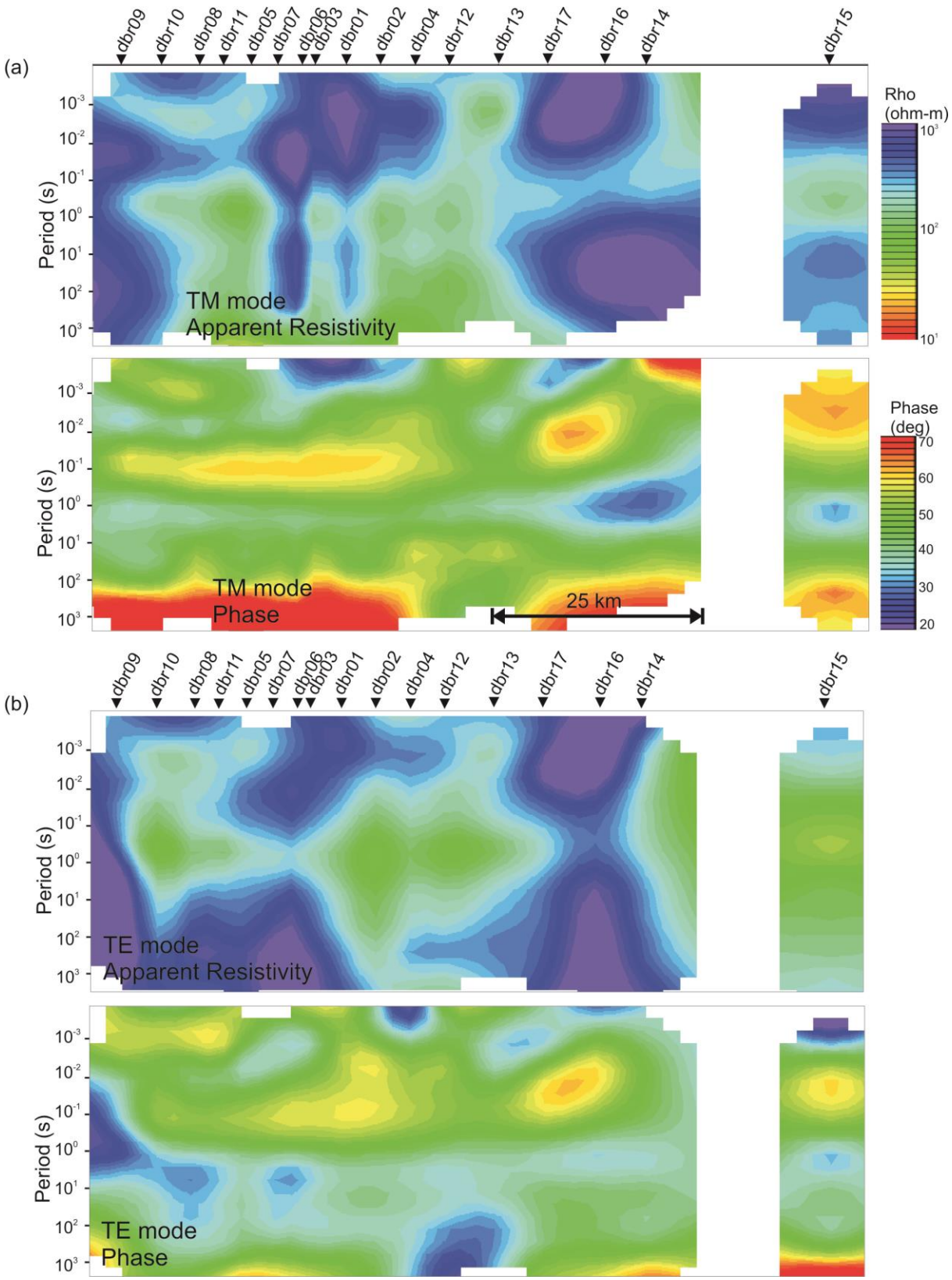

Figure 6 Pseudosections of apparent resistivity and phase along the profile comprising data considered to have an acceptable signal to noise level for data in the (a) TM-mode and (b) TE-mode.

that the electric field data are galvanically distorted by local, near-surface features. Single site decompositions were applied to each of the sites using an error floor set to 3.5%, equivalent to 2° phase, as described in McNeice and Jones (2001). The resulting preferred strike azimuth, with a 90° ambiguity, and the average phase difference between the conductive and resistive directions for one-decade period bandwidth are shown in Figure 5 for periods between 0.001 – 500 s. Where the phase difference between the TE- and TM-modes is minimal (<10°) the data can be considered 1-dimensional, or independent of the geo-electric strike angle. Where the phase difference is larger, the data are more dependent on the strike angle, and 2-D models need to be generated at the appropriate geo-electric strike angle in order to accurately represent the subsurface resistivity structure. In general, at periods between 0.01 – 10 s most of the sites show low phase differences (< 10°), suggesting that the data are approximately 1-D. At shorter periods the phase difference is high at a few sites at the west end of the profile, with a strike angle of ~65° likely resulting for localized near-surface structure. At periods between 0.01 – 0.1 s, although phase differences are small (<15), there is a consistent preferred strike angle of 318 - 342° (with an average of 331°) at all but 3 sites. This angle roughly corresponds to the strike direction of the Franklin dykes, suggesting that the TE-mode runs parallel to -29°. Recalling the ambiguity in strikes of +/- 90°, at periods between 10 – 100 s there is a weak preference for an angle of ~45°. However at periods greater than 100 s there is a fairly consistent preferred strike angle of ~10 - 20° for most of the sites, and which is particularly evident at periods greater than 100 s.

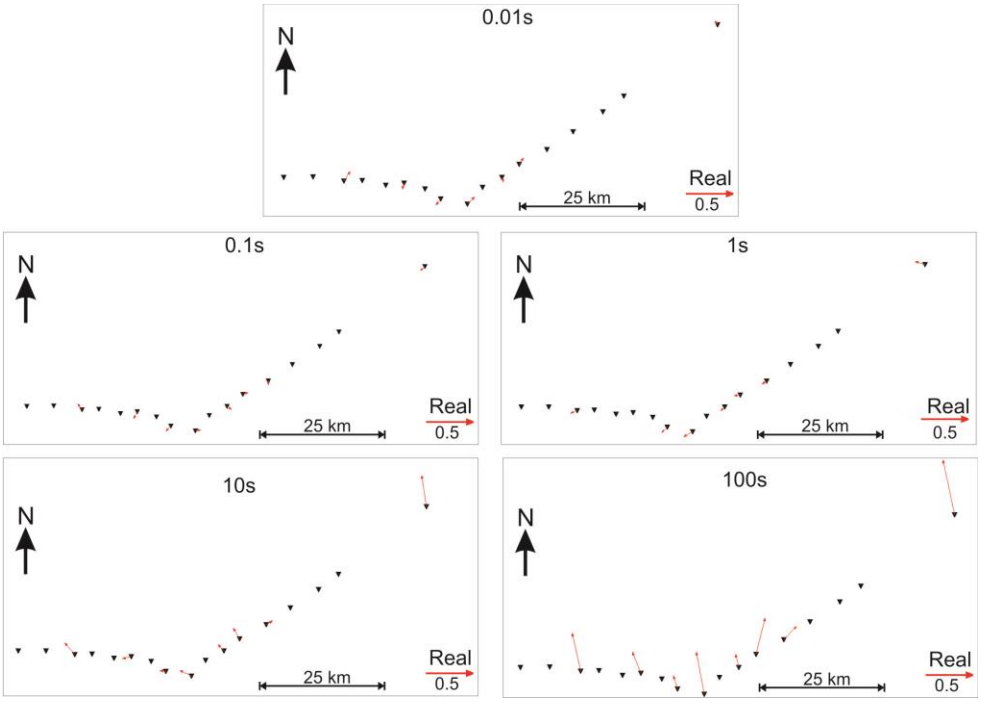

Figure 7 Map view of induction arrows using the Parkinson convention at 5 different periods for all MT sites acquired.

Pseudosections of the phase and apparent resistivity responses for each of the sites along the profile were generated for both the TE- and TM-modes (Figure 6). As apparent resistivities may be affected by static shift, the phase pseudosections are typically observed to determine areas that are 1-D. The phases of the TE and TM-modes shows similar layered structure along the profile to periods of at least 10 s, an indication that the data are largely 1-D.

Where lateral conductivity gradients exist along a profile within the Earth, vertical magnetic fields are created (in a 1-D Earth vertical magnetic fields are non-existent). Induction arrows are the vector representations of the complex ratios of the vertical to horizontal magnetic fields. The Parkinson convention, where real arrows point towards regions of low resistivity, has been used to plot induction vectors at various periods (Figure 7). Induction vectors show very low magnitudes at periods below 10 s, another indication that the data are 1-D. At longer periods, the induction vectors generally point towards the coastline, suggesting that the data are influenced by ocean sea water effects.

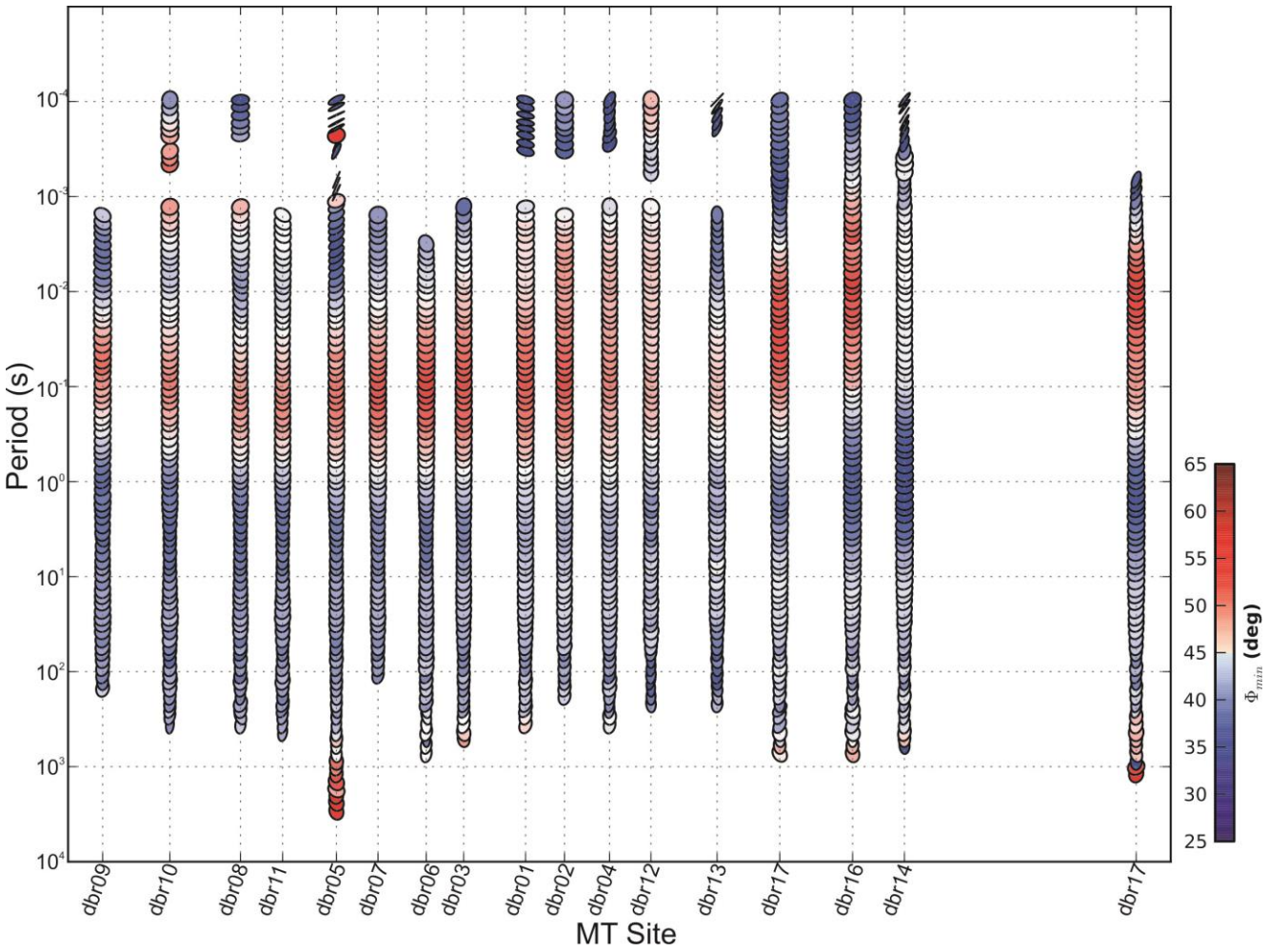

Figure 8 Pseudosection display of MT phase ellipses and phase minimums along the profile. The blue colors represent phase minimums below 45° and the red colors represent phase minimums above 45° .

The dimensionality of the MT data was further assessed using the phase-tensor method of Caldwell et al. (2004). Unlike many other dimensionality estimation methods, this method analyzes only the phase variations because these are unaffected by galvanic distortion associated with near-surface changes in electrical conductivity and the method does not rely upon assumptions that the regional electrical structure is 1D or 2D. Three parameters are used to characterize the phase tensor: the maximum (Φ_{max}) and minimum (Φ_{min}) phase values, and the skew angle (β). The phase tensor is commonly represented as an ellipse, with the long and short axes of the ellipse representing the maximum and minimum phase values respectively (the TE- and TM-modes) and the orientation of the major axis representing the direction of maximum current flow, or geoelectric strike angle. At periods where the phase difference between the TE- and TM-modes is minimal (<10°) the data are deemed one-dimensional (1-D), i.e. independent of geoelectric strike angle and the phase ellipse is a pseudo circle. With the influence of two-dimensionality, the ellipticity increases. Phase tensor ellipses have been plotted in pseudosections for each station along the profile, where the red colours represent phase minimums above 45°, generally indicating a change from resistive to more conductive rocks, and the blue colours below 45°, a change from conductive to resistive units with depth (Figure 8). The phase tensor ellipses are shown as open circles to periods of at least 1 s, and 10 s for most of the eastern sites. At longer periods the ellipses are oriented roughly north-south to NNE. Rose plots of the strike angle for each period band have been generated from the phase tensor ellipses (Figure 9). Rose plots show a large degree of scatter at periods below 1 s, further indicating

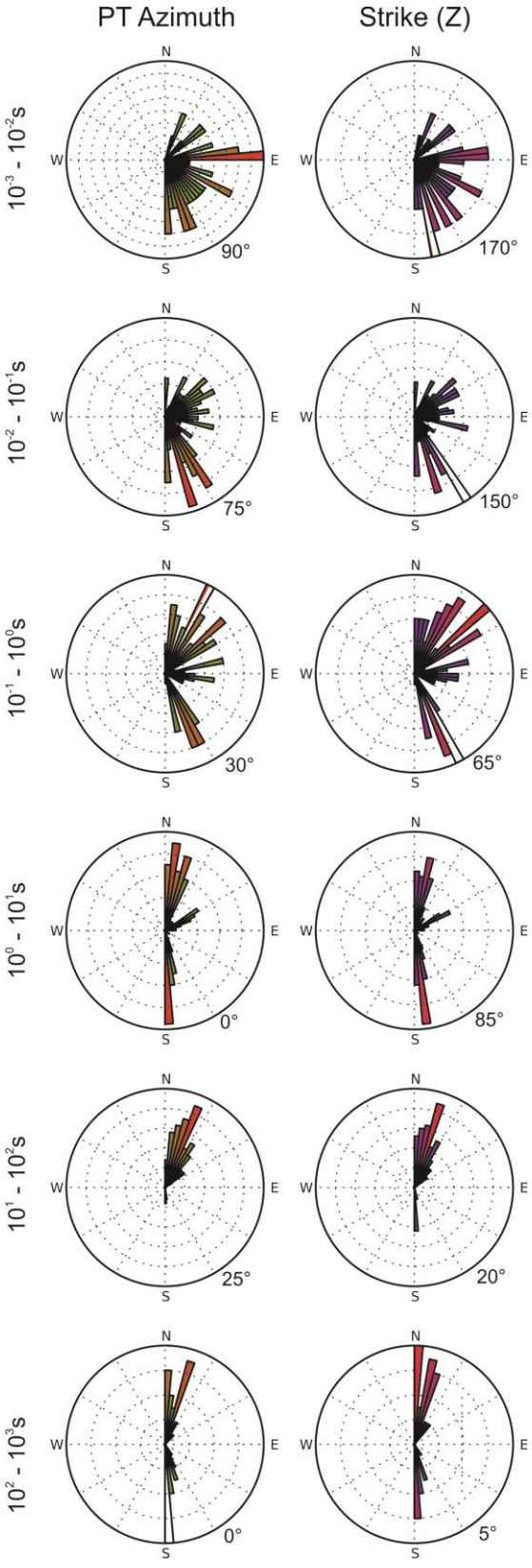

Figure 9 Rose diagrams of phase tensor ellipses and z-strike orientations at 6 decade period bands for all MT sites along the profile.

that the data are 1-D. For periods between 1 – 10 s and 100 – 1000 s, there is a preferred strike of 000°, and from 10 – 100 s the preferred strike is 025°.

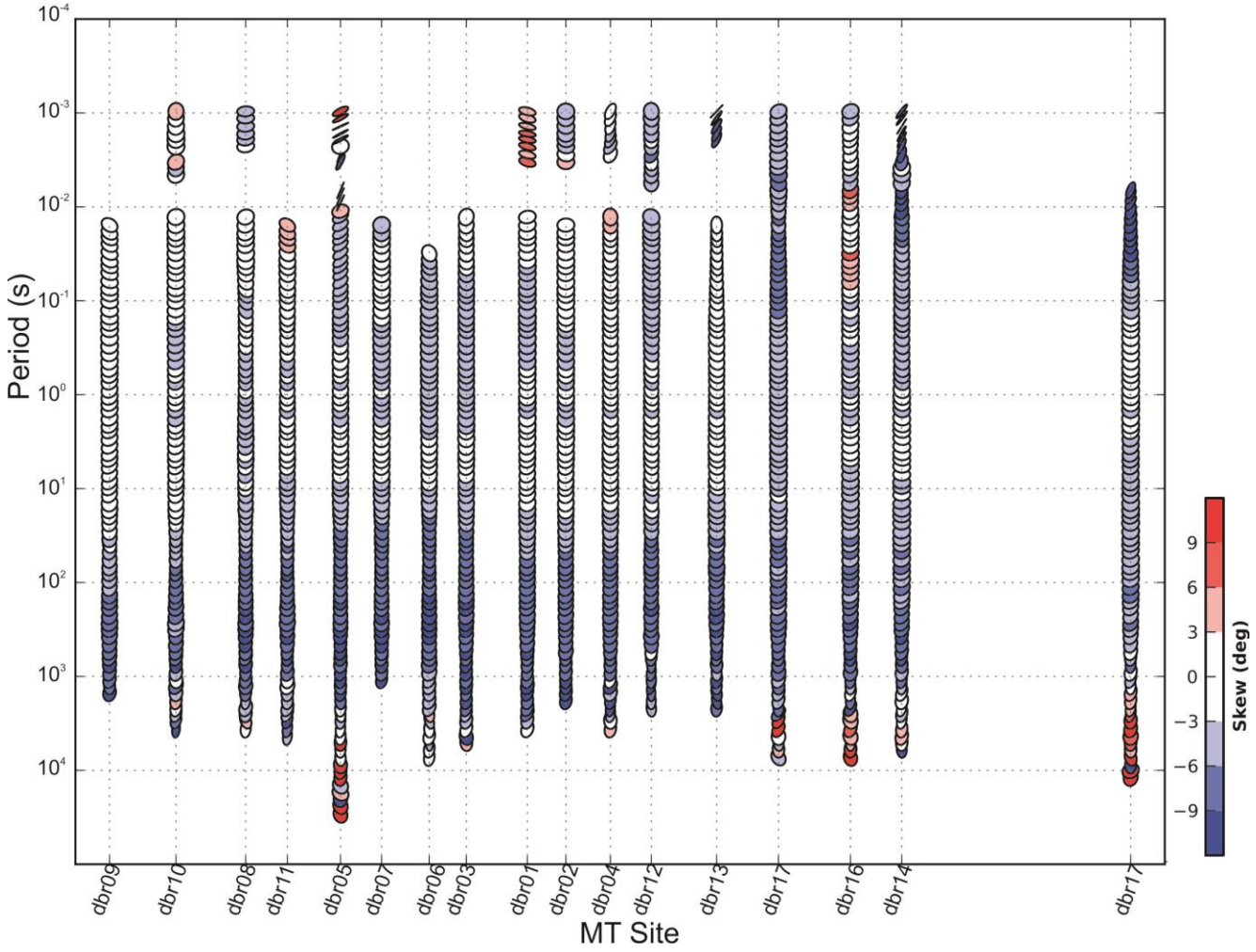

Figure 10 Pseudosection display of MT phase ellipses and skew (β) along the profile. The dark blue color represents a skew value below -5 and the dark red color represent skew value above +5.

A 3D subsurface results in a skewed ellipse with the main axis deflected by an angle β from the symmetry axis. Phase tensor ellipses are plotted in pseudo section with the colour represents the skew value (Figure 10). Blue colours indicates a skew of <-5 and red indicates >+5. Empirically, -5<β<5° means the data should be predominantly 2D. A skew outside this range is likely affected by 3-D characteristics. Along the MT profile, skew values above and below ±6 are observed at periods greater than 20 - 100 s, an indication of 3D effects in the deep structure.

The data have been recalculated at strike angles of 14°, 45°, and 61° based on the decomposition analysis and 0° and 25° based on the phase tensor analysis. Plots of RMS value over the period range for each site and each strike angle are shown in Figure 11. Where the misfit value is < 2, a 2-D model can be generated to adequately represent the data. The geo-electric strike angles that best fit most of the sites over most of the period ranges are 0° and 14°; however, several of the sites at

particular frequencies do not fit the data regardless of the strike angle selected. This is particularly true for the periods shorter than 0.01s, likely a result of the poor data quality in the response curves. Two-dimensional models have been generated along the MT profile with the data recalculated at strikes of -29°, 0°, and 14° to observe how the model resistivity structure varies with azimuth. Periods greater than 10s, typically corresponding to depths in the mid- to lower crust, are too deep to discern easily the 90° ambiguity in the geo-electric strike analysis; however, analysis of skew suggests that these data are influenced by 3D distortion and should not be included in 2D modelling.

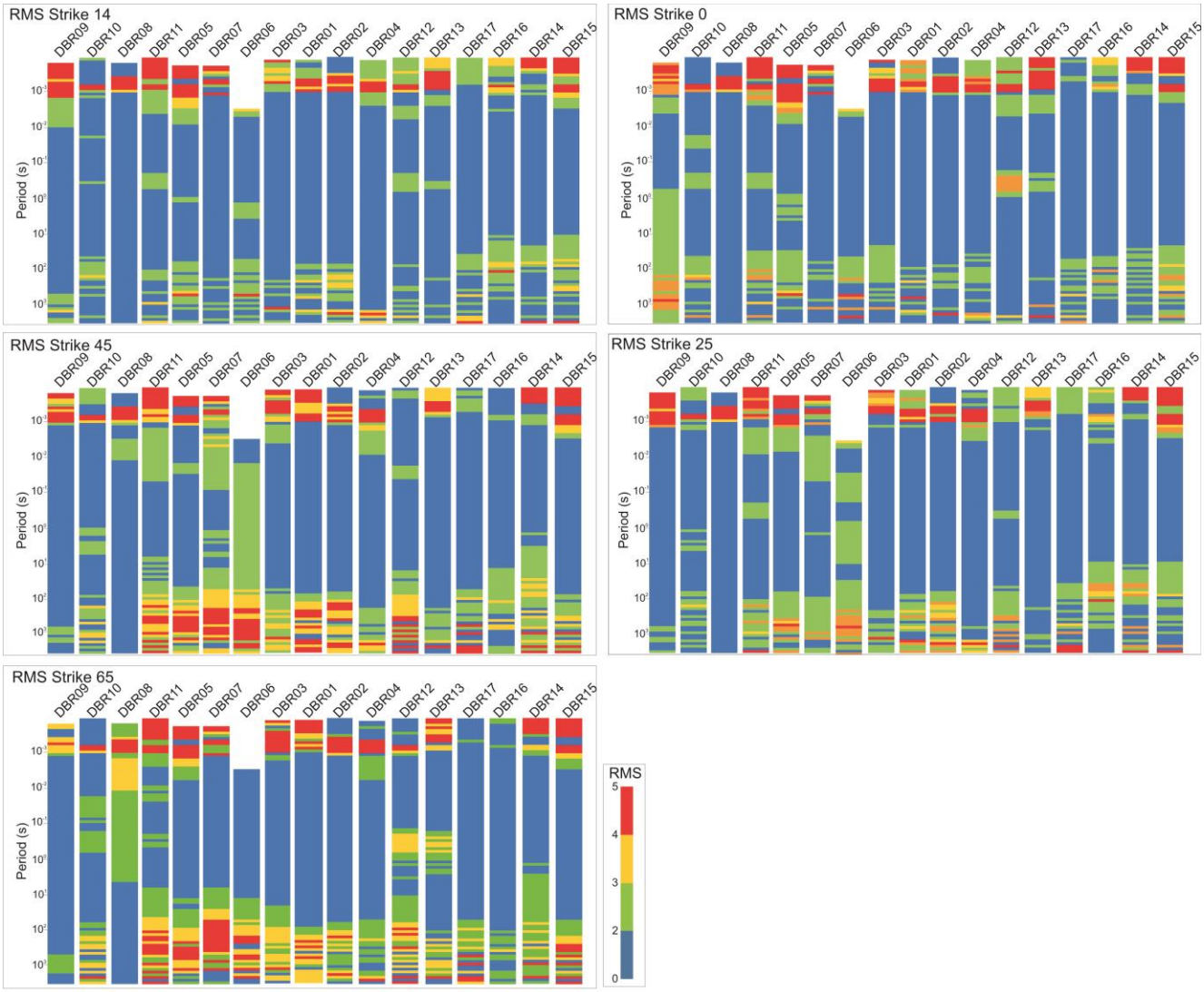

Figure 11 Data misfit values at each site over the whole recorded period range for data along the profile, recalculated at a geo-electric strike direction of 14° (a), 45° (b), 65° (c), 0° (d) and 25° (e).

4.3 Depth estimates

Rough estimates of penetration depths were determined using Schmucker's c-function analysis, which calculates the depth of maximum eddy current flow (Schmucker, 1970). These show that the

data penetration at 300 s is > 100 km for all sites and >300 km for most sites in the xy direction (Figure 12a and b). At 20 s, above which the data are largely 3D, penetration estimates generally greater than 30 km in both the xy and yx directions (Figure 12c and d). Groom-Bailey decompositions identified a weak strike direction of ~61° at periods of 0.01 – 0.1 s. Depth estimates are between 2 – 5 km in both the xy and yx directions at 0.1 s.

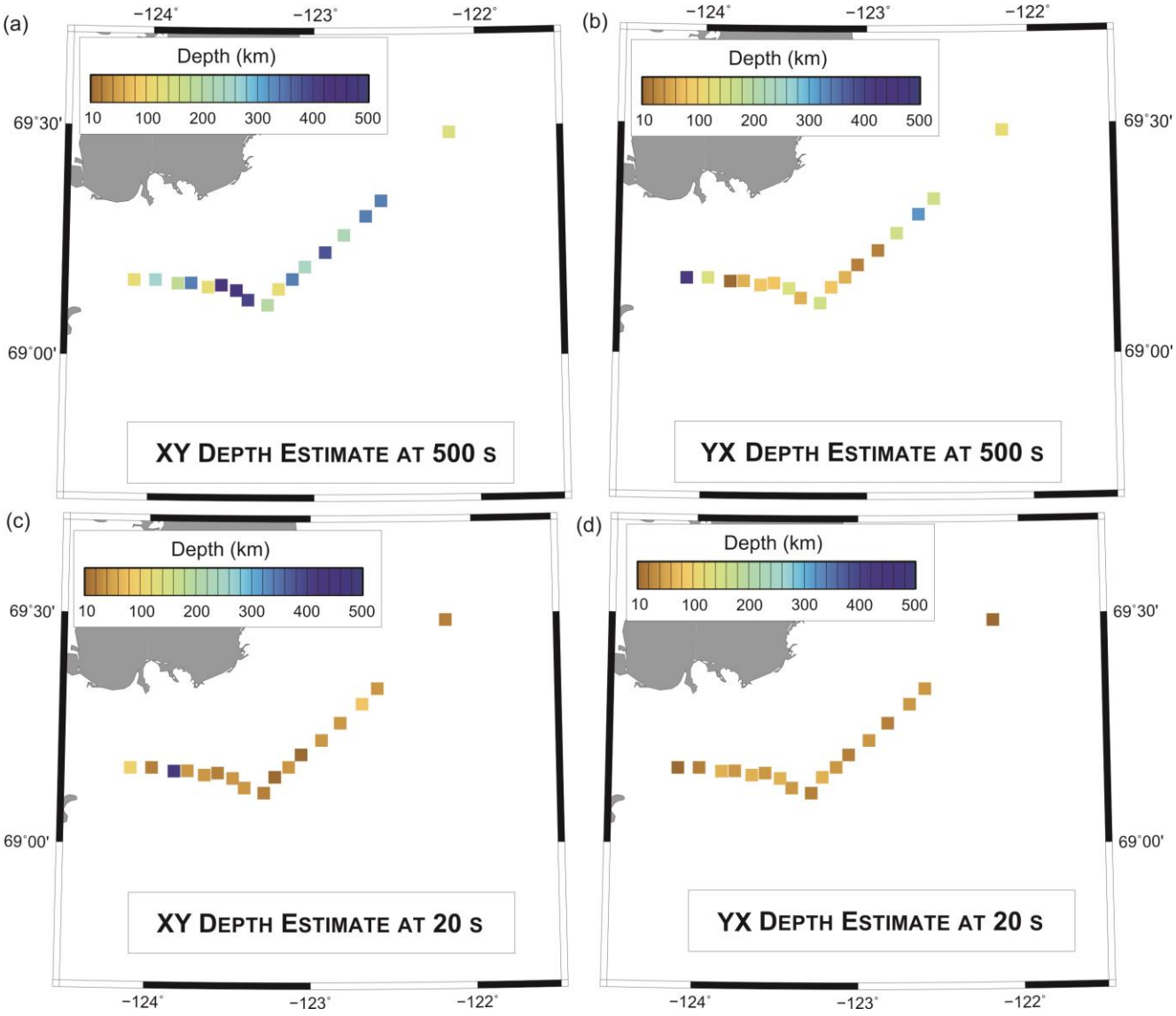

Figure 12 Estimates for maximum penetration depths at periods of 500 s at each site in the measured (a)north-south and (b)east-west directions and at periods of 20 s in the (c) north-south and (d) east-west directions.

4.4 Ocean effects

It is known that the presence of sea water, a near-surface 3-dimensional conductive body, can have significant effects on MT data due to the sharp contrast in resistivity between the land and the ocean (Schmucker, 1970, Menveille et al., 1982). The coastal effects is typically observed in the long period data and the severity of these effects is dependent on the salinity of the sea water, the

conductivity structure of the subsurface, the depth of the ocean, and the proximity of the MT site to the coast (eg. Santos et al., 2001, Pous et al., 2002). In order to assess the coastal effects on this data set, a coarse 3-D mesh was created with ocean resistivity values of 0.3 ohm·m extending to depths of 400m, (approximated from the International Bathymetric Chart of the Arctic Ocean : http://www.ngdc.noaa.gov/mgg/bathymetry/arctic/arctic.html), and a uniform land resistivity value of 500 ohm-m (Figure 13). A forward model then generated synthetic response curves at the recorded site locations. This method of determining coastal effects is an approximation, as the coast line is not exact, the depth and resistivity of the ocean is estimated, and a uniformly resistive earth was used rather than a layered or structured earth. It is therefore only used to illustrate caution in interpreting 2-dimensional models that include long period data near the coast.

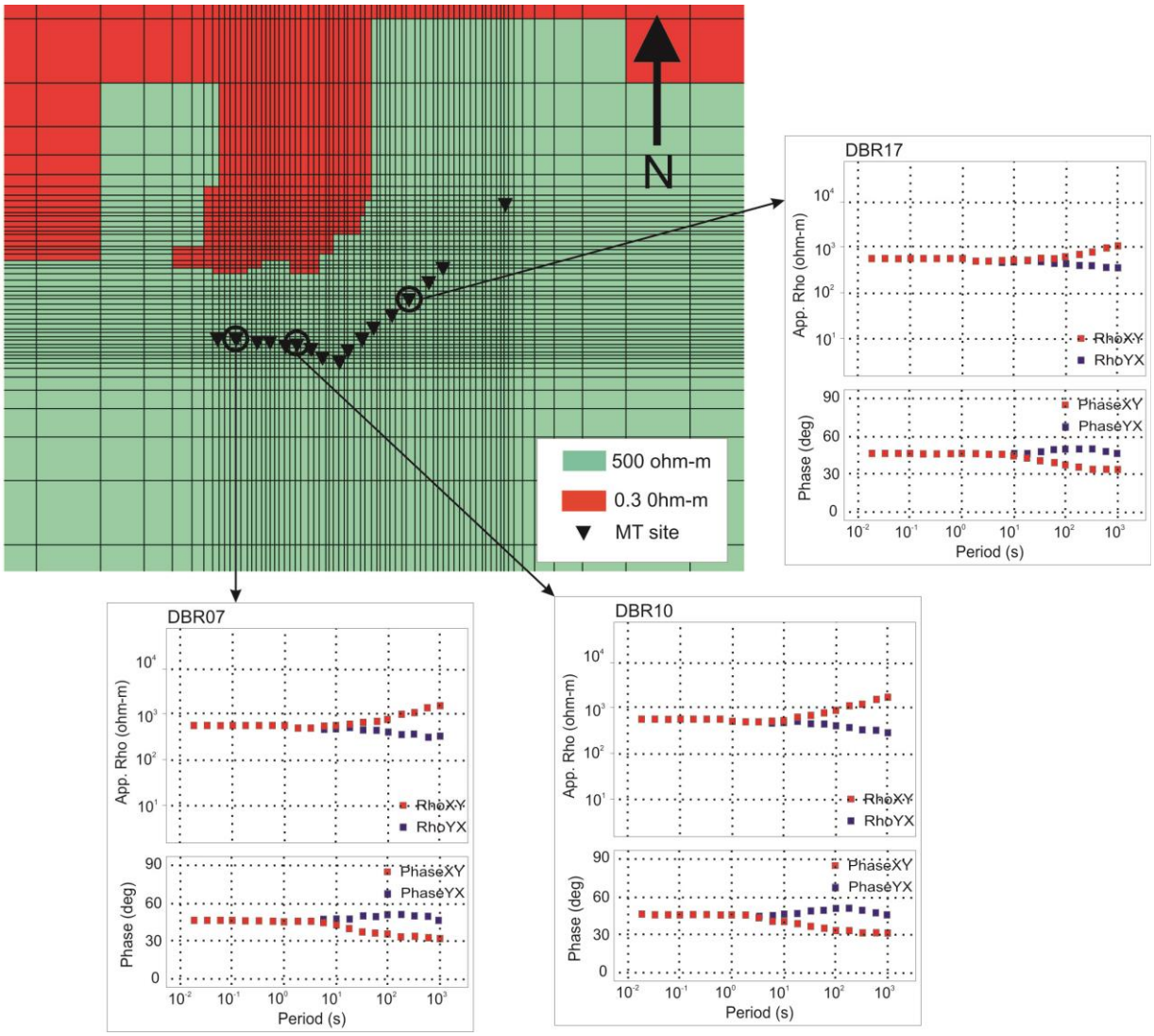

Figure 13 The 3-D mesh of the MT survey area showing the land versus ocean conductivity contrast. Examples of the forward calculated response curves are shown for sites DBR10, DBR07, and DBR17.

The calculated forward response curves show that there could be significant coastal effects at most sites along the profile for periods greater than 20s. This is consistent with induction vectors that point towards the coast and with high skew values. Models have been generated using all data, and omitting data at periods greater that 20 s.

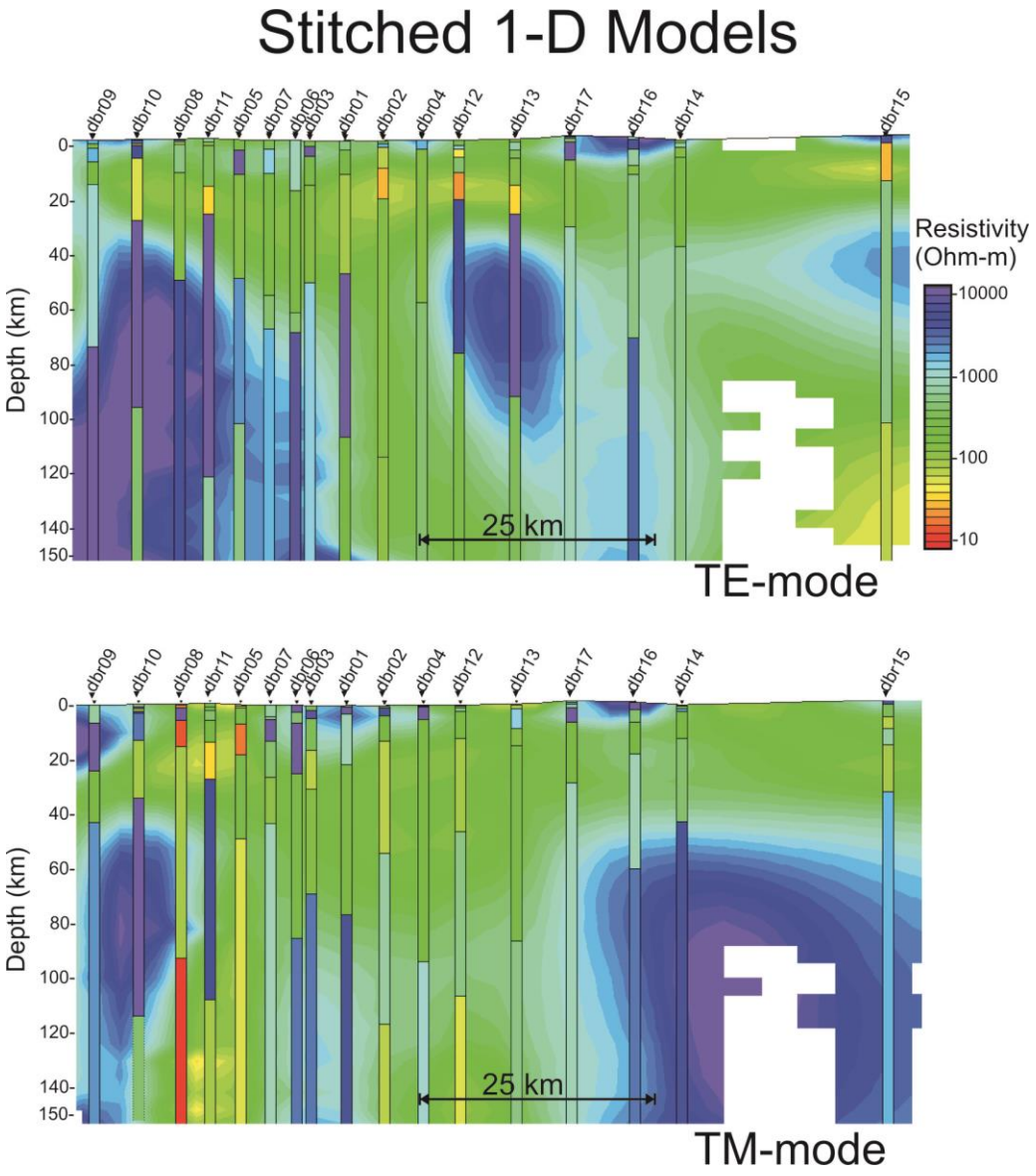

Figure 14 Cross-sections along the profile illustrating the results of 1-dimensional Occam inversions in the TE- (top) and TM- (bottom) modes.

5.0 Data Modeling

The distortion-corrected, regional 2-D responses from sites along the main northwest to southeast profile have been imported into the WinGlink MT interpretation software package at a geo-electric strike angle of -29°, 0°, and 14°. Each site has been manually edited to remove data points with either large error bars or large scatter, as well as phases above 90° or below 0°. Although the

degree of static shift effects on the data cannot be numerically determined, static shift effects arise from a charge build up at the base of near surface conductors and the effect is to raise the apparent resistivity values of the entire response curve. Where one apparent resistivity curve was much higher than another, the curve was dropped to match that of the other curve at the shortest period. This helps to reduce the effect of anisotropic shift, but does not account for the static shift cases were both curves are affected (example of anisotropic data is shown in Figure 4b). Plots of pseudosections of the data (Figure 6) do not show large lateral variations in the apparent resistivities, indicating that static shift effects are minimal.

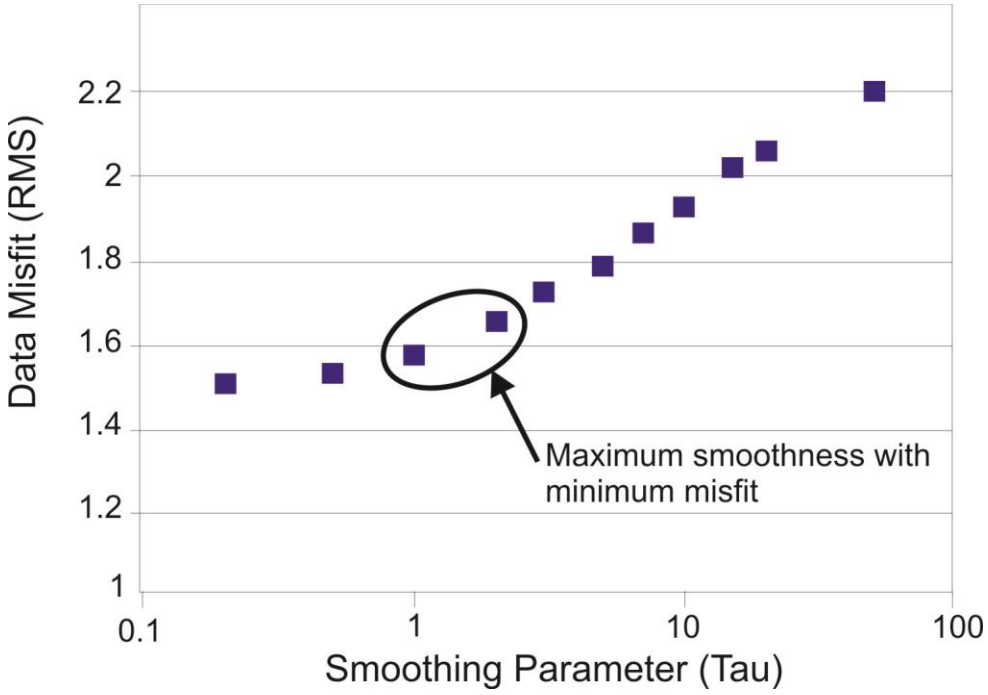

Figure 15 Plots of the trade off between the RMS misfit of the model to the data and the tau value of the inversion after 100 iterations. The black ellipse marks the optimal tau value.

5.1 1-D Models

One-dimensional layered Earth models were generated for each site using Occam's inversion codes as implemented by the WinGlink MT interpretation software package and stitched together to create cross-sections along the MT profiles (Figure 14).

5.2 2-D Models

As is common with many regularized inversion codes, this 2-D code searches iteratively for the smoothest model that best fits the data by attempting to trade off the fit to the observed data (data misfit) with the squared Laplacian (smoothing term) of the horizontal and vertical resistivity gradients. The inversion program searches for the smoothest, best-fit model with the least deviation from the

starting model, which is usually a half space (Mackie and Madden, 1993). This means that the models found represent the minimum structure required to fit the data with an acceptable misfit.

Many different models need to be generated using various combinations of modes and parameters in order to observe the effects of these changes on the model structure and to derive the most robust final model with an appropriate misfit value. Models were initially generated using the entire period range of 0.0001 – 1000 s for the TM and TE-modes. For each model the smoothness parameter, tau, was changed after 100 iterations in order to determine the most appropriate tau value for the data set. Figure 15 illustrates the trade-off between the roughness of the model, defined by the tau parameter, and the fit of the model to the data, RMS. This shows that a tau value of 1 - 3 would result in the smoothest model with the best fit to the data.

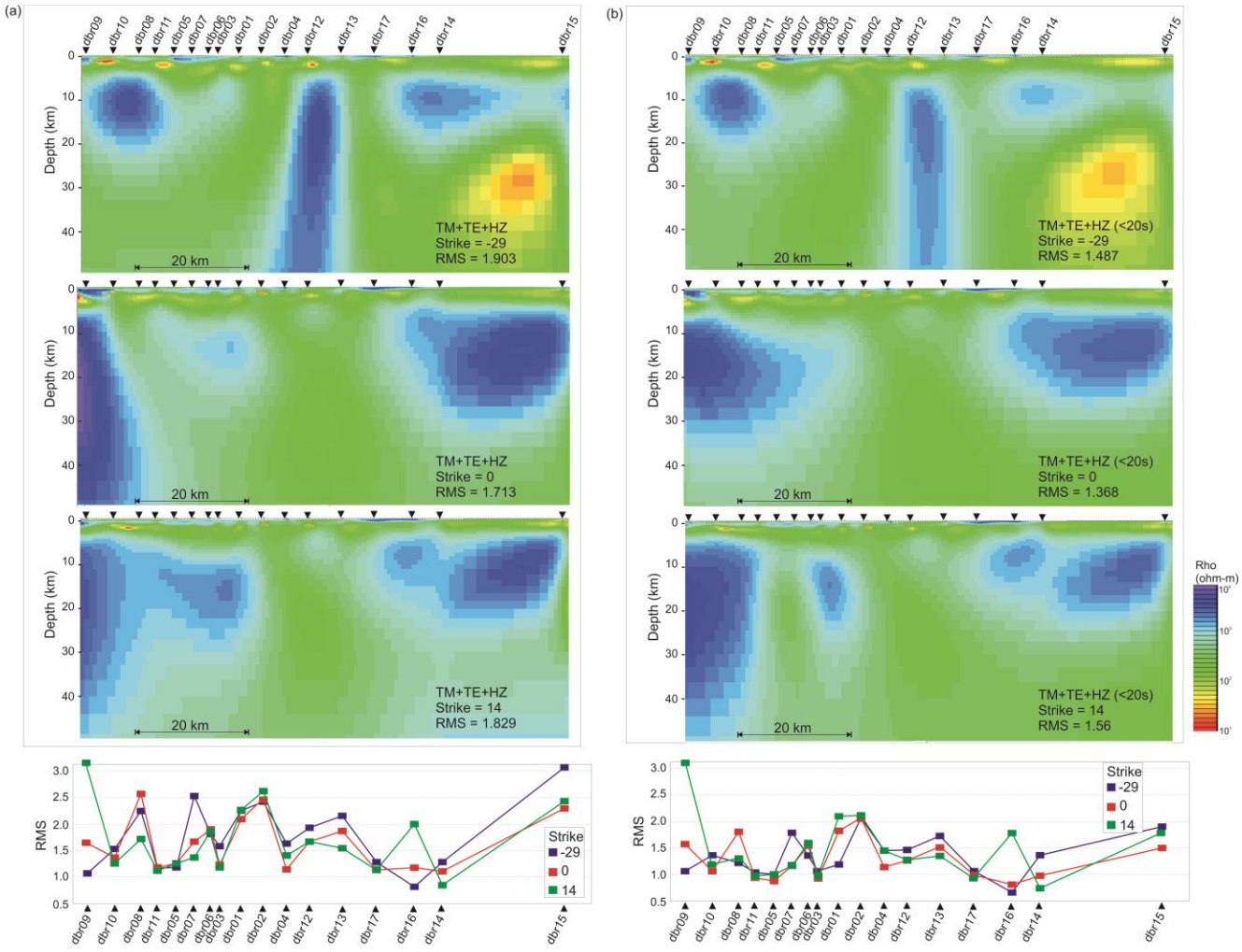

Figure 16 Results of 2D inversion with TE-mode oriented parallel to -29º, 0º, and 14º using (a) data up to 1000 s and (b) data deemed unaffected by ocean sea water, periods up to 20 s. The blue colours represent high resistivity values and the warm colours represent areas of low resistivity.

Models were then generated from the TM- and TE-modes as well as the vertical field data (HZ) at geo-electric strike angles of -29°, 0°, and 14° (Figure 16). Inversions applied a tau value of 3

and included data from the entire period range of 0.0001 – 1000 s as well as the period range estimated to be unaffected by sea water (periods < 20 s). The error floor was set to 20% for the apparent resistivity to account for possible static shift effects, and 7% for the phase. Results show that

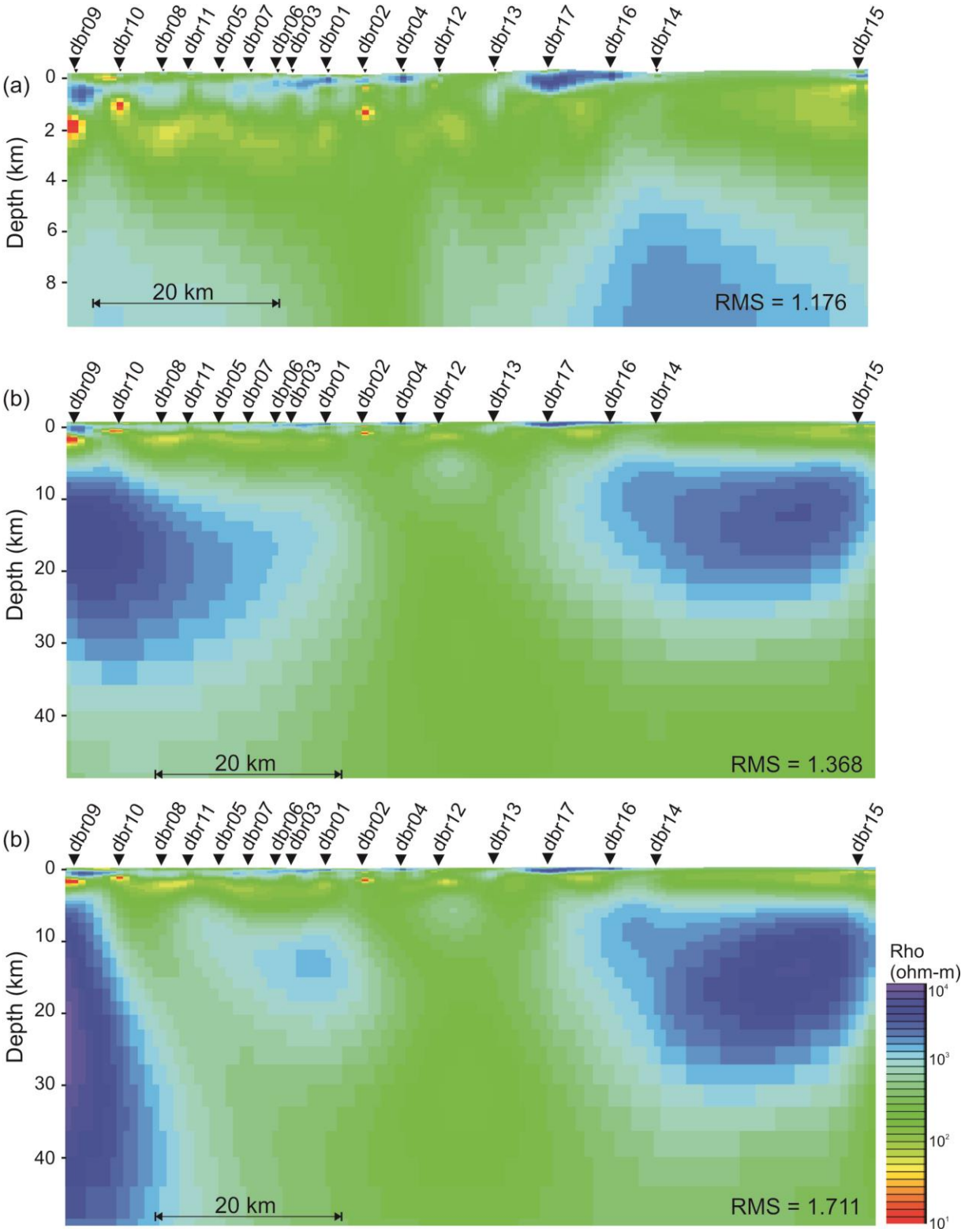

Figure 17 Final resistivity models generated from the MT impedance tensor and vertical field data using periods up to (a) 1s, (b) 20 s, and (c) 1000 s.

regardless of strike direction, the resistivity structure is similar between models to depths of at least 5 km along the entire profile. Large differences in the resistivity structure are observed at depths below 5 km, beneath sites dbr12 and dbr13 in the model generated at -29°. Note that at 65° (-25°) decomposition models showed a poor fit to the data at periods greater than 0.1 s for site dbr12 and at periods of 0.1 – 3 s for site dbr13 (Figure 11). The RMS values after 2D inversion at these sites is highest at a strike angle of -29° and lowest at a strike of 14°. The deep resistivity structure is quite similar between models generated at 0° and 14°, with the lowest overall RMS value of 1.713 using all data and 1.368 using data < 20 s at a geoelectric strike angle of 0°. Preferred models are generated with decomposed data recalculated at a strike angle of 0°.

5.3 **Preferred 2D Models**

Inversions were initiated with a homogeneous half space of 500 ohm·m, a mesh consisting of 77 rows and 135 columns, and a smoothing parameter (tau) of 3. Preferred models were generated at a geoelectric strike angle of 0° using data from the TE-mode, TM-mode, and vertical field transfer function (HZ). Separate models were generated that include periods up to 1 s (Figure 17a) in the attempt to resolve detail in the shallow resistivity structure, periods up to 20 s (Figure 17b) those deemed unaffected by coastal sea water effects, and periods up to 1000 s (Figure 17c). Error floors were set to 20% for the apparent resistivities, 7% for phases and 0.03 for tipper (HZ). Models include topographic information, therefore depths shown are depths below sea level.

Our preferred models have been selected for feature testing and interpretation (Figure 17a and17 b). In the upper 5 km, the preferred resistivity models reveal a thin low resistivity layer (~200 ohm·m) near the surface along the western half of the profile that thickens towards the west up to 350 m beneath the western most extent of the profile. This is underlain by a more resistive layer (1000 - 2000 ohm·m) that is roughly 1 km thick and dips slightly towards the west. Beneath the resistive layer, there is a prominent low resistivity layer (~10 – 200 ohm·m) along the entire length of the profile that extends from the surface beneath sites dbr012 and dbr013 and dips westward beneath the resistive layer. This low resistivity layer varies in thickness from 1 – 3 km along the profile. These results are consistent with those observed along the TAMT profiles.

The deeper structure, in general, shows high resistivities of (>1500 ohm·m) at depths between 5 – 30 km in the eastern half of the profile and up to 40 km in the western half below which resistivities decrease to < 500 ohm-m. The area of exception lies beneath sites dbr002 – dbr013 where

an anomalous near vertical zone of low resistivities (~200 ohm·m) is observed between 5 – 30 km depth. This zone coincides with the eastern extent of the Darnley Bay anomaly.

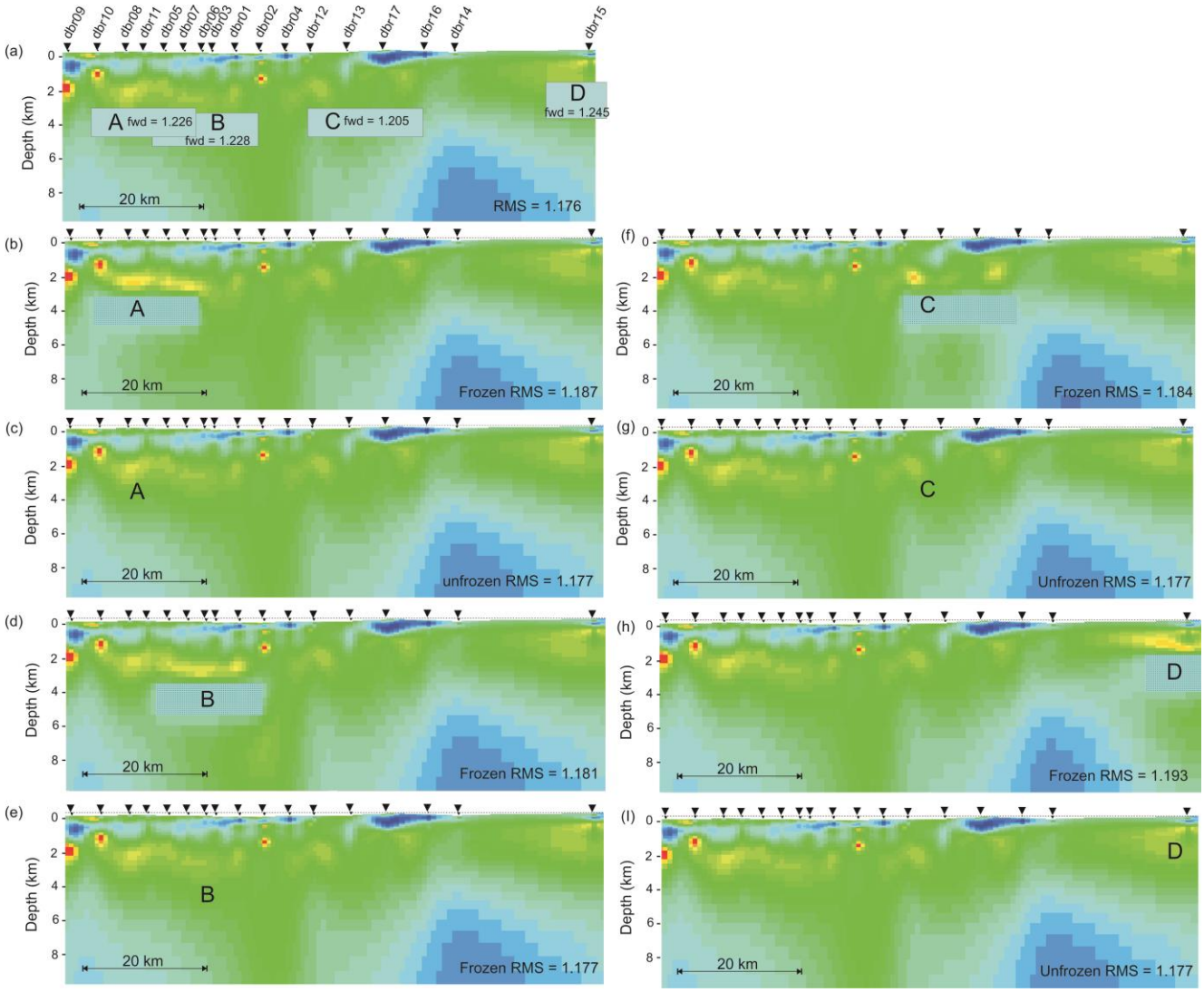

Figure 18 Results of feature testing within the upper 5 km of the resistivity model. (a) shows the lettered features that were altered and the resulting RMS values after forward inversion; (b) new model and RMS value with feature A frozen; (c) new model with feature A unfrozen; (d) new model with feature B frozen; (e) new model with feature B unfrozen; (f) new model with feature C frozen; (g) new model with feature C unfrozen; (h) new model with feature D frozen; and (I) new model with feature D unfrozen.

5.4 **Feature testing**

To test the reliability of the preferred resistivity models produced by the inversion, 'feature testing' was undertaken on various distinct conductive and resistive zones. This method involves removing and replacing resistivity values of a group of cells with those of the adjacent area. A forward calculation is first performed on the data to assess the change in RMS value, then the resistivity of the altered area is 'frozen' and the inversion process re-started. This means the inversion algorithm is forced to try and match the observations using conductivity variations outside this area. This form of

test is designed to see whether conductivity variations in another part of the model can be used to fit the data, i.e. does there need to be a zone of anomalous conductivity in the area being tested. The second type of feature test allows the modeling algorithm to modify values within the test zone ('unfrozen') to see if the anomalous zone reappears and if so how its geometry is affected. This test is less rigorous than the first in terms of the presence or absence of a feature but allows the reliability of the feature's geometry to be assessed, i.e. does it re-appear in the same form as in the original model.

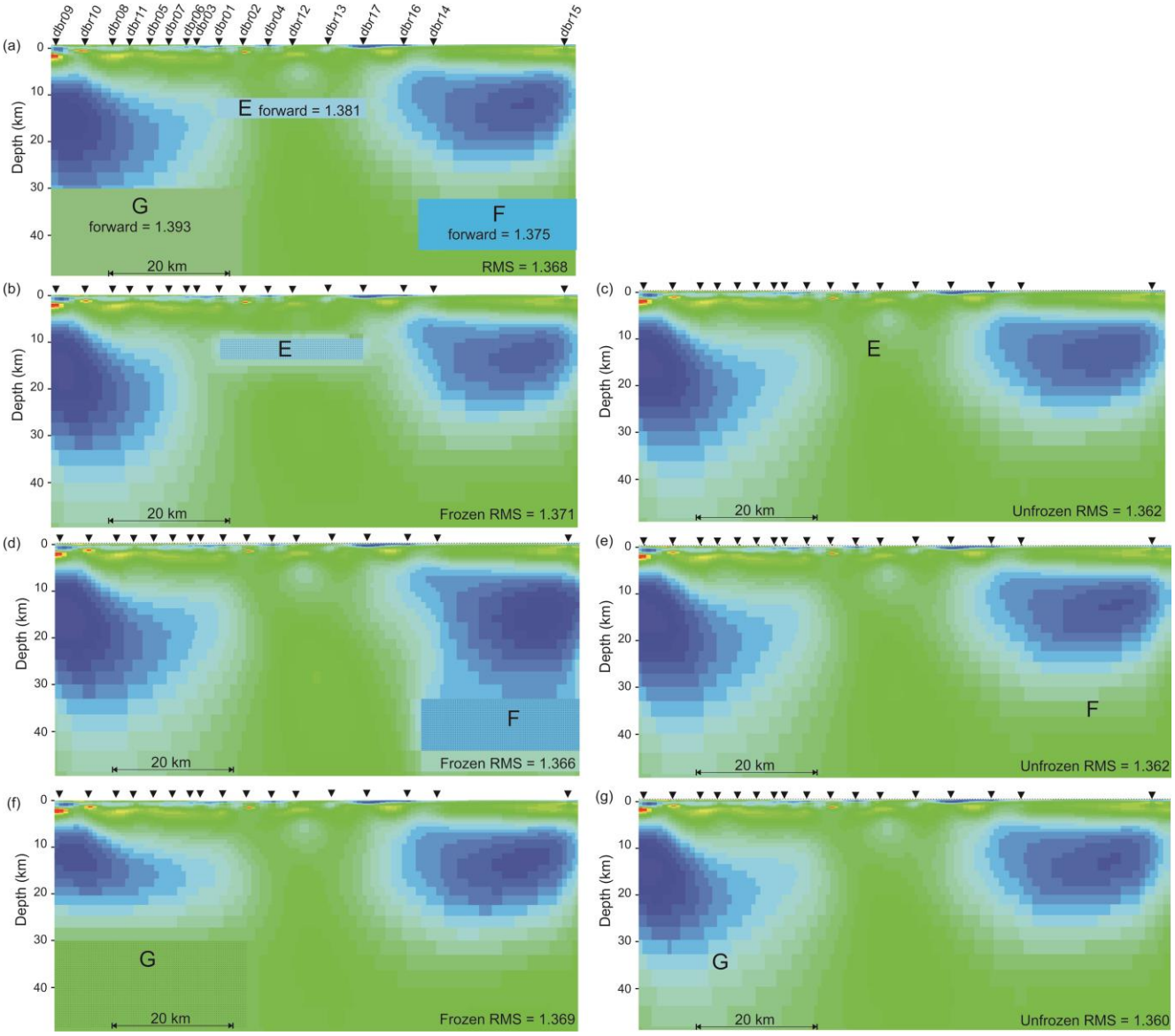

Figure 19 Results of feature testing in the deep structure of the resistivity model. (a) shows the lettered features that were altered and the resulting RMS values after forward inversion; (b) new model and RMS value with feature E frozen; (c) new model with feature E unfrozen; (d) new model with feature F frozen; (e) new model with feature F unfrozen; (f) new model with feature G frozen; (g) new model with feature G unfrozen.

Feature testing was applied to several areas of the preferred resistivity models, both within the shallow resistivity structure and the deeper image. MT imaging is typically good at resolving the top of a low resistivity layer, but poor at resolving the transition from low resistivity to high resistivity

with depth. The resolution of the lower limit of the low resistivity layer imaged was tested by altering the original preferred model and inserting four resistive blocks along the profile, labeled from west to east as features A, B, C, and D (Figure 18). In each case, a forward calculation of the altered model yielded a higher overall RMS value with increases of 2.4 – 5.8%. This is an indication that the data are sensitive to the structure at these depths. With the areas frozen, the inversions were not able to generate a model with the RMS value as low as the original model, however features B and C had RMS values that were incrementally increased by 0.3 % and 0.7 % respectively (Figure 18d, and f). Unfrozen, in every case, the models reverted back to the original resistivity structure and original RMS value (Figure 18c, e, g, and i). This testing indicates that the base of the low resistivity layer is fairly well resolved in the preferred MT model.

At greater depths, the near vertical low resistivity zone was tested by inserting a resistive block, feature E, connecting the east and west mid-crustal resistive sections (Figure 19a, b, and c). A forward inversion yielded an increase in RMS of 0.9%. With the area frozen, the inversion was able to reduce the RMS to that of the original model by lowering the resistivities of the cells both east and west of the frozen area. Unfrozen, the model returned to the original resistivity structure. These tests indicate that a low resistivity zone is required by the data, but that the position and resistivity value are largely unresolved.

Finally, the sensitivity of the data to the deep structure was tested by inserting a resistive block between 25 – 33 km, consistent with values observed at shallower depths, beneath the eastern end of the profile a lower resistivity block consistent with values observed at greater depths, between 32 - 42 km depth beneath the western end of the profile labeled as features F and G respectively (Figure 19). A forward inversion of the altered models resulted in an increase in RMS value of 0.4% for feature F, and 1.7% for feature G. In both cases, with the areas frozen, the RMS values were reduced to values equal to the original model with little change to the surrounding cells (Figure 19b, d, and f). With the areas unfrozen, the models reverted to the original resistivity structure with an improved RMS value (Figure 19c, e, and g). These results indicate that there is minimal sensitivity of the MT data to the resistivity at structure > ~30 km.

6.0 Interpretation and Discussion

Interpretations of the resistivity structure revealed by the MT data are illustrated for the upper 8 km (Figure 20a) and for the deeper structure beneath the profile (Figure 20b). The near surface low

resistivity layer in the western half of the profile is interpreted to represent the Pleistocene glacial cover. Thicknesses of up to 350 m are consistent with information from drill hole DBR001.With a resistivity value of ~200 ohm·m, estimated for the Pleistocene glacial cover, the minimum depth that can be resolved at periods of 0.0001s is ~70 m. This means that the data are not sensitive to structure above 70 m depth, and may not image thin near surface layers. The cover rocks may extend further to the east as shown in the geologic map, but are too thin to be detected. The westward dipping resistive layer likely represents the silicified carbonates of the Cambrian Ronning Group and/or Franklin Mountain Formation, noted between 377 – 1167 m in drill hole DBR001. Consistent with shales, mudstones, and sandstone, values of 10 – 200 ohm·m observed across the entire profile in the low resistivity layer are interpreted to represent sedimentary rocks of the Shaler Supergroup. These interpretations for the upper 5 km are consistent with the results and interpretations of the TAMT northern line (Goldak and Olsen, 2015). Two small zones of high resistivity are noted beneath sites dbr017 and dbr016, and beneath site dbr015. Cambrian carbonates are not exposed in these areas and the cause of these resistive units remains uncertain.

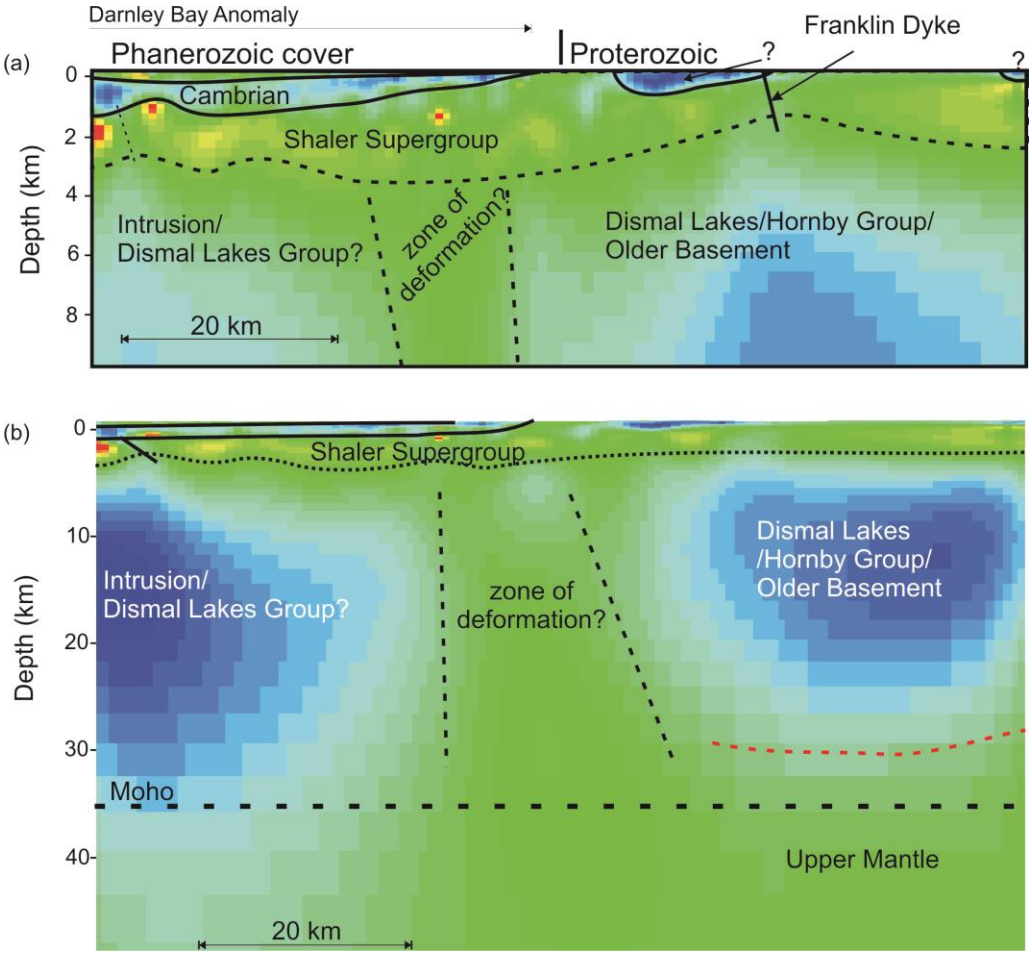

Figure 20 Geologic interpretation of resistivity structure derived from modelling the MT data, Mopho depth fo 36 km is from Snyder (pers. comm.).

At mid-crustal depths the vertical low resistivity zone has values of ~200 ohm·m (Figure 17b and Figure 20b). These values are too high to be caused by fluids, metallic mineralization, or graphitic films each typically < 10 ohm·m. This area may represent a zone of deformation related to faulting along the western margin of the Brock Inlier, which coincides with the eastern margin of the Darnley Bay anomaly. NW-trending faults were mapped along the Hornaday River by Cook and Aitken (1969). The zone is imaged as being over 15 km wide, possibly due to the oblique orientation of the profile with respect to the plane of the fault zone. This is the only feature that varied significantly with differing model parameters. Model testing has shown that a vertical low resistivity zone is required by the data; however, the specific location and resistivity value within the zone may not be well resolved.

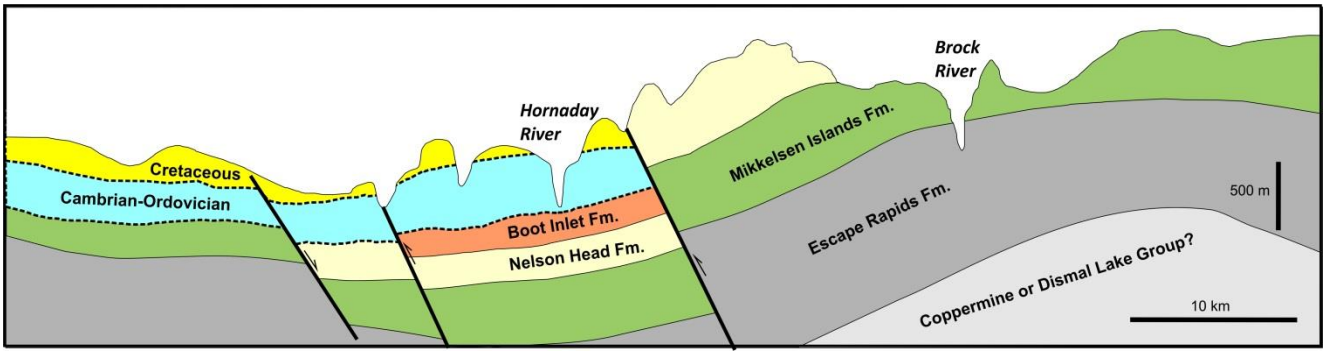

Figure 21 Geological cross section along MT transect between DBR08 and DBR17, based on regional geology (compiled by Okulitch, 2000) and spot observations made during recent regional reconnaissance mapping (Rainbird et al., 2015b)..Thin solid lines are depositional contacts and dashed lines are unconformities. The thick solid lines are faults, with latest stage of displacement indicated by arrows. Vertical exaggeration approximately 20x.

The MT data are not able to distinguish the Dismal Lakes and Hornby Bay groups from the older Archean basement rocks. This is somewhat surprising as basement rocks have been shown to have resistivity values >10,000 ohm-m, not observed along this profile (e.g. Spratt et al., 2009). Additionally, the similar resistivity values east and west of the low resistivity zone suggest that the MT data are not able to distinguish the Dismal Lakes and Hornby Bay Groups from the Darnley Bay anomaly. The depth and thickness of the Shaler Supergroup low resistivity layer is fairly constant along the entire length of the profile, indicating that the top of the Darnley Bay anomaly lies at greater depths and does not intrude these sedimentary sequences. This suggests that, if the Darnley Bay anomaly is related to a dense mafic magmatic intrusion, it is not the Franklin large igneous province, which does intrude the Shaler Supergroup (Jefferson et al., 1994). We note also that dykes imaged on the total magnetic field aeromagnetic map (Figure 2) and along strike with dykes mapped elsewhere as Franklin (e.g. Cook and Aitken 1969), appear to cut across the anomaly and are therefore younger than it. There is a better possibility that the anomaly is related to the 1270 Ma Mackenzie large igneous province (LeCheminant and Heaman, 1989), including the Coppermine flood basalts, which underlie

much of the region to the east of Brock Inlier. Although the sensitivity of the data has shown to be poor at depths greater then ~30 km, a decrease in resistivities from high to moderate values at ~32 km depth is consistent with estimates for the crust mantle boundary beneath the Slave craton (Spratt et al., 2009, Snyder pers. comm.). For preliminary comparative purposes, a geological cross-section (Figure 21) has been generated for the region. Of note are interpreted faults that coincide with the zone of deformation identified in the resistivity structure derived from modelling the MT data. These faults and the multiple stages of movement/reactivation implied by the stratigraphy of the faulted panels are inferred from geological relationships observed mainly along the Hornaday and Brock rivers and mapping by Cook and Aitken (1969). A reverse fault with several hundred metres displacement and lying on strike with the one shown in the middle of the cross section is exposed in the valley of a west-flowing tributary of the Hornaday, south of the transect (see Figure 1).

7.0 Conclusions

The 2015 AMT and broadband MT data have imaged the 2D resistivity structure of the crust beneath the Darnley Bay anomaly and Brock Inlier within the Northwest Territories. Strike and dimensionality analysis reveal that the data are largely 1-dimensional to periods of at least 0.1 s, with a preferred geo-electric strike angle of 0º for the deeper structure. It is shown that distortion effects due to the presence of coastal sea water affect the data at periods greater than 20 s.

The models reveal a thin near-surface low resistivity layer along the western half of the profile, interpreted as Mesozoic and Cenozoic cover sediments that thicken up to 350 m beneath the western most MT site. These are underlain by a resistive layer that is ~1 km thick and interpreted as Paleozoic silicified carbonates that have a slight westward dip. The siliciclastic and carbonate sedimentary rocks of the early Neoproterozoic Shaler Supergroup are imaged 1 – 3 km thick low resistivity layer along the entire length of the profile.

At mid-crustal depths, resistivities generally are high with values of ~1000 ohm·m. The MT models do show a resistivity contrast between the Dismal Lakes-and Hornby Bay sedimentary rocks, older basement rocks, or the suspected Darnley Bay mafic intrusion. The intrusion is imaged beneath the Shaler Supergroup and its magnetic expression is cut by dykes of Franklin age so it is older than 1.0 Ga. A low resistivity zone marks the eastern extent of the Darnley Bay anomaly and is interpreted as a deformation zone that extends to at least 20 km depth. The exact nature of these discontinuities is the subject of ongoing 3-D modelling of the data to account for the variability of the electrical strike and effects of the ocean.

7.0 Acknowlegements

Our work is funded by the Geological Survey of Canada's Geomapping for Energy and Minerals (GEM) initiative. Thank-you to the residents of the Hamlet of Paulatuk and Diane Ruben (Paulatuk HTC) for facilitating community engagement meetings. Special thanks to Maya March and Renee Wissink (Parks Canada) for help with field logistics, Jonah Nakimayak and Francis Wolki (Wildlife monitors+), Scott McLeod (helicopter pilot) and Kevin Vickers (Discovery Mining-expediting). Logistical support provided through the assistance of the Polar Continental Shelf Project (NRCan) by Great Slave Helicopters and Summit Aviation.

References

Aspler, L.B., Pilkington, M., and Miles, W.F., (2003). Interpretations of Precambrian basement based on recent aeromagnetic data, Mackenzie Valley, Northwest Territories; *Geological Survey of Canada, Current Research*, 2003-C2, 13 pg.

Baragar, W. R. A., and Donaldson, J. A., 1973, Coppermine and Dismal Lakes map areas: Geological Survey of Canada, Paper 71-39, 20p.

Caldwell, T.G., Bibby., H.M, and Brown, C. (2004). The magnetotelluric phase tensor: Geophysical Journal International, v. 158, p. 457–469.

Cook, D. G., and Aitken, J. D., 1969, Erly Lake, District of Mackenzie (97A), Geological Survey of Canada Map 5-1969, Scale 1:250,000.

Cook, D.G., and MacLean, B.C. (2004). Subsurface Proterozoic stratigraphy and tectonics of the western plains of the Northwest Territories, *Geological Survey of Canada, Bulletin* 575.

Goldak, D. K. (2014). Darnley Bay Project: Results of a Transient Magnetotelluric Survey

Goldak. D. K., and Olsen, R.W. (2015). New developments in audio-magnetotelluric exploration: Case study from Darnley Bay area, N.W.T.; *CSEG Recorder*, v. 40, n. 2, p. 22 – 27.

Groom, R.W., and R.C. Bailey (1989). Decomposition of magnetotelluric impedance tensors in the presence of local three-dimensional galvanic distortion; *Journal of Geophysical Research,* v. 94, p. 1913 – 1925.

Heaman, L.M., LeCheminant, A.N., and Rainbird, R.H. (1992). Nature and timing of Franklin igneous events, Canada: Implications for a Late Proterozoic mantle plume and the break up of Laurentia; *Earth and Planetary Science Letters*, v. 109, p. 117 – 131.

Jefferson, C.W., Hulbert, L.J., Rainbird, R.H., Hall, G.E.M, Gregoire, D.C., and Grinenko, L.I., (1994). Mineral resource assessment of the Neoproterozoic Franklin Igneous Events of Arctic Canada: Comparison with the Permo-Triassic Noril'sk-Talnakh Ni-Cu-PGE deposits of Russia; *Geological Survey of Canada, Open File* 2789.

Jones, A.G. and H. Jödicke (1984). Magnetotelluric transfer function estimation improvement by a coherence based rejection technique (EM1.5), in Abstract Volume: *54th Society of Exploration Geophysics Annual General Meeting,* Atlanta, Georgia, USA, SEG Extended Abstracts v. 3, p. 51–55.

Jones, A.G., and Spratt, J. (2002). A simple method for deriving the uniform field MT responses in auroral zones. *Earth Planets Space,* 54, p443 – 450.

Jones, T.A., Jefferson, C.W., and Morrell, G.R., (1992). Assessment of mineral and energy resource potential in the Brock Inlier – Bluenose Lake area, N.W.T.; *Geological Survey of Canada, Open File* 2434.

Mackie, R.L., and Madden, T.R. (1993). Three-dimensional magnetotelluric inversion using conjugate gradients; *Geophysical Journal International*, v. 115, p. 215 – 229.

MacLean, B.C., and Cook, D.G., (1992). The influence of Proterozoic structures on the development of Laramide structures, northern Interior Plains, Northwest Territories, Canada; *Bulletin of Canadian Petroleum Geology*. v. **40**, p. 207 – 221.

Mareschal, M., (1986). Modelling of natural sources of magnetospheric origin in the interpretation of regional induction studies: a review, *Surv. Geophys.*, **8**, 261–300.

McNeice, G.W., and Jones, A.G. (2001). Multisite, multifrequency tensor decomposition of magnetotelluric data. *Geophysics*, v. 66, p. 158 – 173.

Menvielle, M.J.C., Rossignal, P. and Tarits, P. (1982). The coast effect in terms of deviated electric currents: A numerical study. *Physics of the Earth and Planetary Interiors*, v. 28, p. 118 – 128.

Okulitch, A.V. (2000). Geology, Horton River, Northwest Territores-Nunavut. *Geological Survey of Canada, Open File* 3845, doi:10.4095/211240.

Pous, J., Heise, W., Schegg, P.A., Munoz, G., Mart, J., and Soriano C. (2002). Magnetotelluric study of the Las Canadas caldera (Tenerife, Canary Islands): structural and hydrogeological implications; *Earth and Planetary Science Letters*, v. 204, p. 249 – 263.

Rainbird, R.H., Jefferson, C.W., Hildebrand, R.S., and Worth, J.K. (1994). The Shaler Supergroup and revision of Neoproterozoic stratigraphy in the Amundsen Basin, Norwest Territories; *Current Research* 1994-C, Geological Survey of Canada p. 61 – 70.

Rainbird, R.H., Jefferson, C.W., and Young, G.M. (1996). The early Neoproterozoic sedimentary succession B of northwest Laurentia: Correlations and paleographic significance; *Geological Society of America Bulletin*, v. 108, p. 454 – 470.

Reford, S. (2012). 43-101 Technical report on the Darnley Bay anomaly, for Darnley Bay Resources Ltd.

Santos, F.A.M., Nolasco, M., Almeida, E.P., Pous, J., and Mendes-Victor, L.A. (2001). Coast effects on magnetic and magnetotelluric transfer functions and their correction: application to MT soundings carried out in SW Iberia; *Earth and Planetary Science Letters*, v.186, p. 283-295.

Schaeffer, A. J. and Lebedev, S., 2014, Imaging the North American continent using waveform inversion of global and USArray data ,; *Earth and Planetary Science Letters*, v.402, p. 26–41.

Schmucker, U. (1970). Anomalies of geomagnetic variations in the southwestern United States, *Bulletin of Scripps Institute of Oceanography*, v. 13, 165 p.

Spratt, J.E., Jones, A.G., Jackson, V.A., Collins, L., and Avdeeva, A. (2009). Lithospheric geometry of the Wopmay Orogen from a Slave craton to Bear Province magnetotelluric transect; *Journal of Geophysical Research*, v.114, no. B)1101, doi: 10.1029/2007JB005326.

Stacey, R.A. (1971). Interpretation of the gravity anomaly at Darley Bay, N.W.T.; *Canadian Journal of Earth Sciences*, v.8, p. 1037 – 1042.

Wight, D.E. and F.X. Bostick (1981). Cascade decimation — a technique for real time estimation of power spectra; in Proceedings: Institute of Electrical and Electronic Engineers; *International Conference on Acoustics, Speech, and Signal Processing*, Atlanta, Georgia, USA, 30 March 1981, p. 626–629.

Vye, L.R., 1972, Seismic Reflection Survey of Darnley Bay Area on the Arctic Coast, *Arjay Kirker Resources Ltd*.

Table 1 MT site locations, electric line lengths, and magnetic field information used for data processing.

Site Name	Data Range	Latitude	Longitude	MTU#	Ex length (m)	Ey length (m)	Hx Coil	Hy Coil	Hz Coil
DBR01b	AMT	69.111590	-123.284190	1494	43.1	45.1	DBR02	DBR02	MT8H7059
DBR01b	BBMT	69.111590	-123.284190	1494	43.1	45.1	COIL1289	COIL1294	MT8H7059
DBR02b	AMT	69.146160	-123.217540	1492	51.7	44.5	AMTC1170	AMTC1173	-
DBR02b	BBMT	69.146160	-123.217540	1492	51.7	44.5	DBR01	DBR01	-
DBR03a	AMT	69.122250	-123.403270	1496	50.8	47.7	DBR02	DBR02	MT8H7319
DBR03a	BBMT	69.122250	-123.403270	1496	50.8	47.7	DBR01	DBR01	MT8H7319
DBR04a	AMT	69.167780	-123.132450	1495	47.1	44.1	DBR02	DBR02	MT8H7322
DBR04a	BBMT	69.167780	-123.132450	1495	47.1	44.1	DBR01	DBR01	MT8H7322
DBR05a	AMT	69.150100	-123.647290	1494	52.0	53.6	DBR08	DBR08	-
DBR05a	BBMT	69.150100	-123.647290	1494	52.0	53.6	COIL1289	COIL1294	-
DBR06a	BBMT	69.142590	-123.473820	1495	52.5	48.9	DBR05	DBR05	-
DBR07a	AMT	69.154690	-123.566310	1496	51.6	51.8	DBR08	DBR08	MT8H7509
DBR07b	BBMT	69.154690	-123.566310	1496	51.6	51.8	DBR05	DBR05	MT8H7509
DBR08a	AMT	69.157890	-123.832760	1497	49.3	43.8	AMTC1170	AMTC1173	MT8H7322
DBR08b	BBMT	69.157890	-123.832760	1497	49.3	43.8	DBR05	DBR05	MT8H7322
DBR09a	AMT	69.164590	-124.099240	1495	50.0	40.6	DBR08	DBR08	-
DBR09b	BBMT	69.164590	-124.099240	1495	50.0	40.6	DBR05	DBR05	-
DBR10a	AMT	69.165560	-123.969050	1497	50.9	53.6	AMTC1170	AMTC1173	-
DBR10a	BBMT	69.165560	-123.969050	1497	50.9	53.6	DBR11	DBR11	-
DBR11a	AMT	69.150910	-123.751060	1494	47.5	50.8	DBR12	DBR12	-
DBR11a	BBMT	69.150910	-123.751060	1494	47.5	50.8	COIL1289	COIL1294	-
DBR12a	AMT	69.195120	-123.057130	1496	48.6	53.0	AMTC1172	AMTC1172	MT8H7509
DBR12a	BBMT	69.195120	-123.057130	1496	48.6	53.0	DBR11	DBR11	MT8H7509
DBR13a	AMT	69.226540	-122.932570	1495	52.2	51.2	DBR12	DBR12	MT8H7322
DBR13a	BBMT	69.226540	-122.932570	1495	52.2	51.2	DBR11	DBR11	MT8H7322
DBR14a	AMT	69.338520	-	1497	50.3	52.1	DBR16/17	DBR16/17	-

			122.588910						
DBR14a	BBMT	69.338520	-122.588910	1497	50.3	52.1	DBR15	DBR15	-
DBR15a	AMT	69.486950	-122.166250	1494	48.6	48.8	DBR16/17	DBR16/17	MT8H7319
DBR15a	BBMT	69.486950	-122.166250	1494	48.6	48.8	COIL1289	COIL1294	MT8H7319
DBR16a	AMT	69.304790	-122.682980	1496	51.5	54.2	AMTC1170	AMTC1173	-
DBR16a	BBMT	69.304790	-122.682980	1496	51.5	54.2	DBR15	DBR15	-
DBR17a	AMT	69.263610	-122.817360	1495	51.2	54.5	AMTC1172	AMTC1171	-
DBR17a	BBMT	69.263610	-122.817360	1495	51.2	54.5	DBR15	DBR15	

Appendix A.

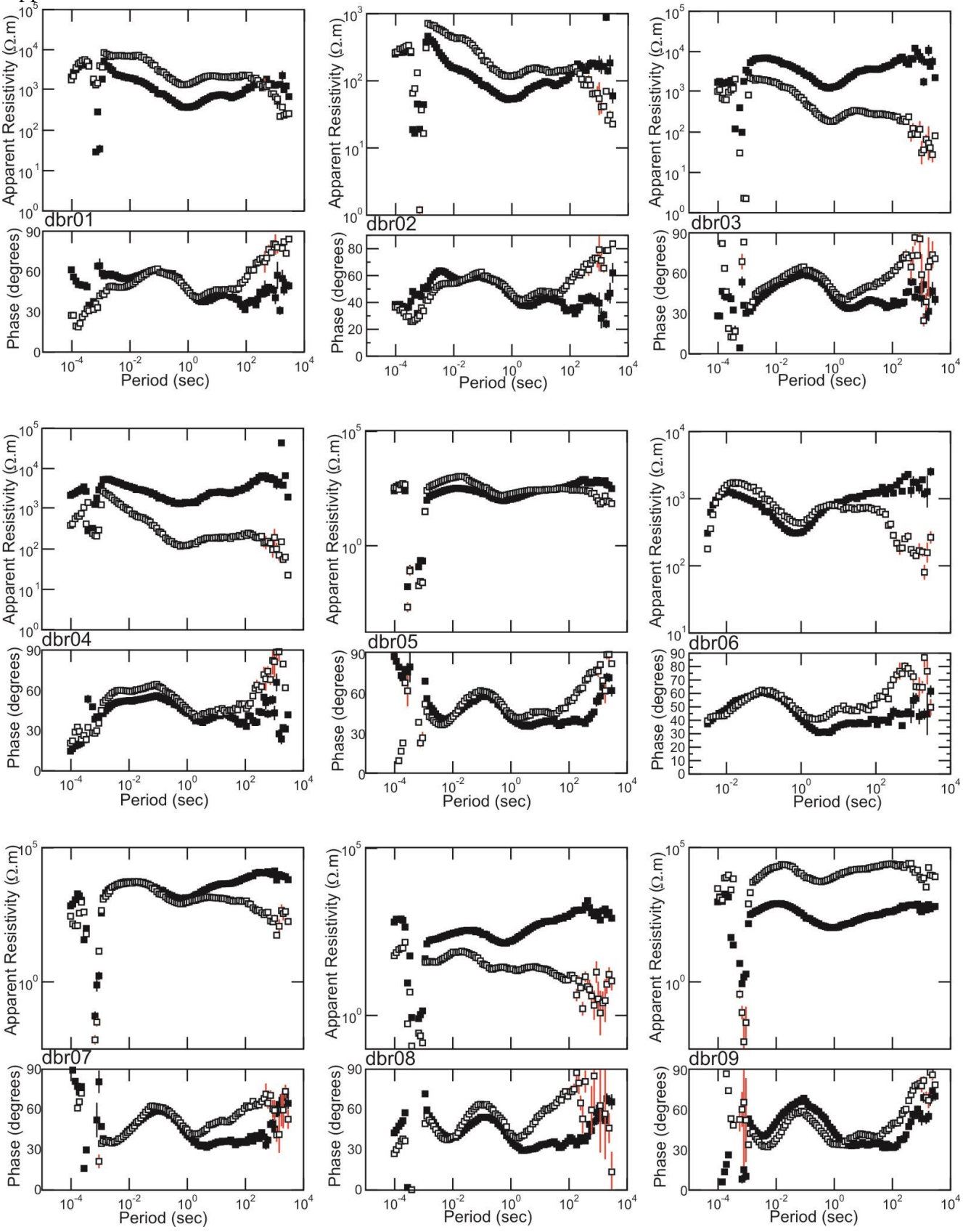
dbr01
dbr02
dbr03
dbr04
dbr05
dbr06
dbr07
dbr08
dbr09
Apparent Resistivity (Ω.m)
Phase (degrees)
Period (sec)

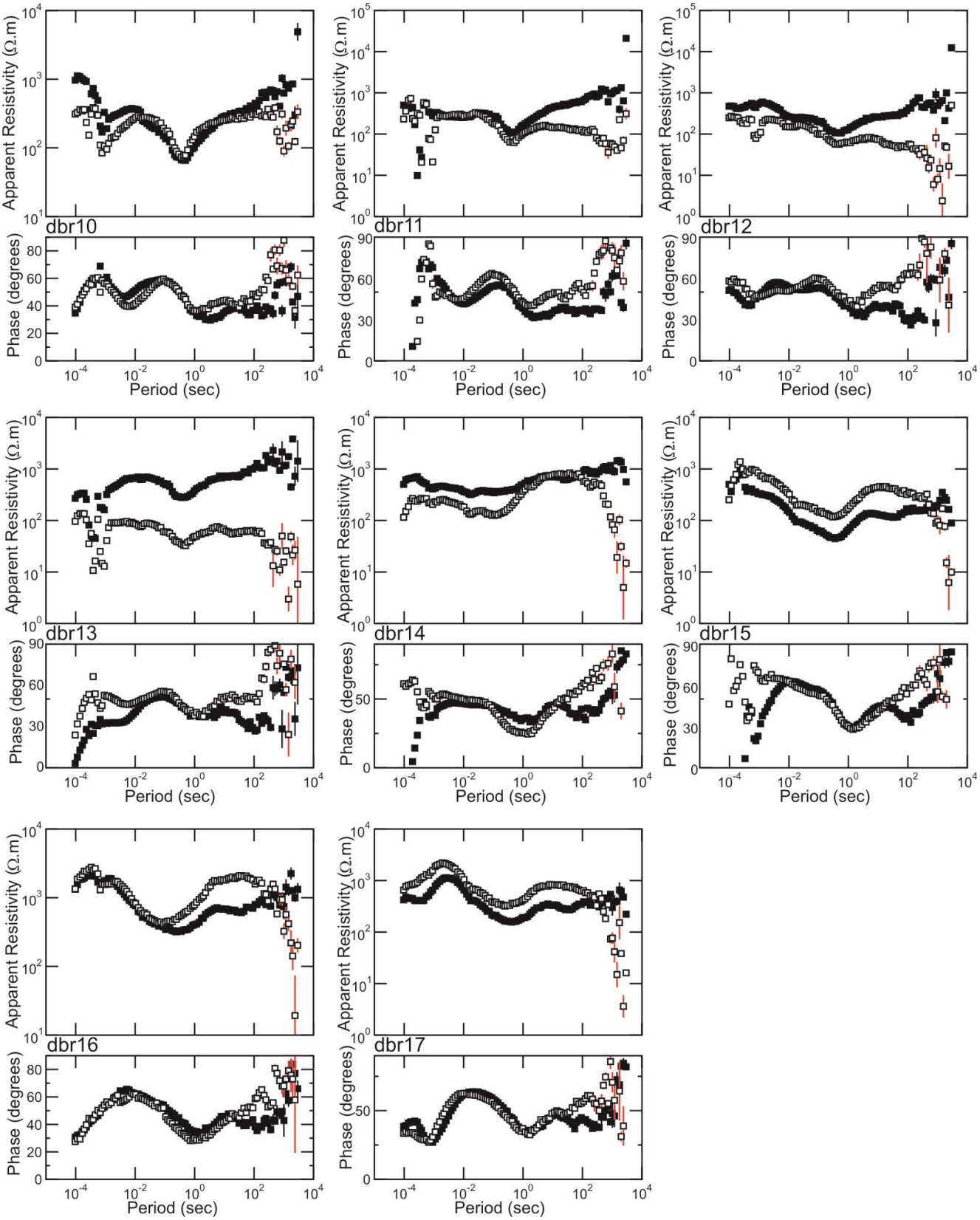
dbr10
dbr11
dbr12
dbr13
dbr14
dbr15
dbr16
dbr17
Apparent Resistivity (Ω.m)
Phase (degrees)
Period (sec)

Appendix B - Magnetic field values (nT) recorded by Space Weather Canada near Cambridge Bay, Nunavut.

Orange cells highlight the times where Hourly Range X, or Z are > or = 200 or the maximum rate of change of X or Z are > or = 40.

Blue rows highlight suspect hours where all above conditions are met.

Date	Hour	Hourly ranges			Hourly mean			Maximum rate of change			Standard deviation		
		X	Y	Z	X	Y	Z	X	Y	Z	X	Y	Z
8-1-2015	1	32	111	46	4629	378	58343	6	11	7	6	37	13
8-1-2015	2	130	111	63	4657	334	58350	14	13	13	34	35	17
8-1-2015	3	34	81	101	4721	432	58357	6	9	9	7	17	32
8-1-2015	4	41	34	25	4743	433	58391	7	5	4	11	8	8
8-1-2015	5	220	228	175	4660	352	58425	68	59	52	59	59	40
8-1-2015	6	100	143	101	4731	377	58385	18	11	14	22	45	31
8-1-2015	7	36	57	56	4737	452	58392	5	9	10	8	13	13
8-1-2015	8	19	38	19	4750	457	58418	4	5	3	5	10	5
8-1-2015	9	25	40	21	4747	459	58428	4	6	7	7	11	4
8-1-2015	10	24	47	65	4734	440	58457	5	5	7	6	14	13
8-1-2015	11	19	45	34	4753	484	58463	9	7	2	5	13	10
8-1-2015	12	53	28	34	4763	481	58448	7	4	5	13	8	8
8-1-2015	13	41	54	42	4736	502	58457	7	11	5	8	17	12
8-1-2015	14	63	52	83	4734	535	58473	10	8	9	13	15	21
8-1-2015	15	96	37	90	4673	528	58520	13	9	12	29	8	29
8-1-2015	16	222	80	107	4665	537	58502	21	7	25	70	24	28
8-1-2015	17	187	36	217	4661	567	58586	47	11	22	50	10	60
8-1-2015	18	283	157	317	4534	578	58515	32	27	46	81	34	82
8-1-2015	19	241	130	235	4631	501	58364	60	35	40	60	40	53
8-1-2015	20	150	169	114	4705	483	58378	29	31	26	32	43	24
8-1-2015	21	122	111	82	4724	514	58381	28	21	17	33	31	18
8-1-2015	22	131	116	105	4759	514	58320	25	26	17	27	24	27
8-1-2015	23	54	76	124	4754	471	58318	13	16	25	14	15	34
8-1-2015	24	164	92	126	4720	457	58286	18	11	12	55	23	34
8-2-2015	1	91	110	62	4657	430	58324	10	10	3	24	31	18
8-2-2015	2	106	88	61	4641	309	58341	22	15	12	30	21	16
8-2-2015	3	49	77	41	4689	376	58316	6	6	6	15	24	9
8-2-2015	4	35	56	59	4728	413	58354	6	3	4	9	15	17
8-2-2015	5	24	25	31	4722	431	58393	3	5	2	6	7	10
8-2-2015	6	24	45	15	4730	438	58413	3	3	2	6	16	3
8-2-2015	7	15	13	16	4745	461	58417	2	4	2	4	3	3

8-2-2015	8	73	100	263	4751	424	58457	23	8	23	15	29	77
8-2-2015	9	84	116	184	4752	403	58567	18	15	19	23	31	48
8-2-2015	10	47	50	94	4748	463	58488	7	8	9	13	16	22
8-2-2015	11	40	32	33	4746	493	58440	7	2	4	11	8	9
8-2-2015	12	36	35	51	4724	490	58456	5	4	5	9	9	10
8-2-2015	13	65	53	40	4744	485	58504	10	5	4	19	14	11
8-2-2015	14	78	56	46	4739	538	58527	14	7	6	20	14	10
8-2-2015	15	80	44	81	4670	550	58606	11	7	12	23	14	21
8-2-2015	16	119	58	190	4605	531	58593	17	12	19	36	13	65
8-2-2015	17	208	173	283	4580	561	58527	53	25	30	50	44	84
8-2-2015	18	132	55	59	4637	516	58390	22	16	14	30	13	14
8-2-2015	19	31	42	70	4707	491	58398	15	8	17	8	9	15
8-2-2015	20	43	112	88	4709	519	58367	8	13	14	10	36	28
8-2-2015	21	67	66	77	4717	471	58381	9	11	9	18	21	22
8-2-2015	22	142	70	241	4717	480	58322	13	12	24	37	22	86
8-2-2015	23	133	37	97	4714	491	58296	9	9	17	31	9	35
8-2-2015	24	81	46	109	4741	485	58296	8	6	17	26	12	29
08-03-15	1	55	45	102	4745	486	58362	9	11	13	11	10	33
08-03-15	2	58	53	89	4745	447	58348	4	4	6	15	19	33
08-03-15	3	76	70	65	4676	397	58338	11	7	10	25	20	17
08-03-15	4	126	65	59	4690	427	58344	17	12	9	43	19	16
08-03-15	5	15	59	25	4745	439	58381	3	2	2	4	18	6
08-03-15	6	48	28	60	4749	416	58412	4	4	5	12	8	18
08-03-15	7	100	63	114	4752	391	58506	13	12	20	26	17	27
08-03-15	8	24	45	46	4750	420	58470	5	9	6	5	13	14
08-03-15	9	24	24	11	4746	458	58453	4	3	2	7	6	3
08-03-15	10	17	31	20	4742	463	58459	4	3	2	4	7	5
08-03-15	11	32	37	30	4729	493	58474	5	4	6	9	12	6
08-03-15	12	31	23	45	4734	498	58453	3	3	6	8	5	9
08-03-15	13	107	75	50	4749	500	58497	6	6	7	37	18	11
08-03-15	14	34	92	70	4840	519	58544	4	8	6	9	26	23
08-03-15	15	84	47	72	4788	553	58480	16	6	4	20	13	23
08-03-15	16	176	30	102	4672	567	58498	17	7	11	58	8	30
08-03-15	17	164	116	84	4660	509	58423	34	23	33	35	24	19
08-03-15	18	76	41	59	4681	470	58418	20	14	24	18	11	13
08-03-15	19	67	56	32	4693	467	58414	19	17	8	12	15	7
08-03-15	20	58	85	54	4715	471	58408	12	18	9	15	21	15
08-03-15	21	77	83	126	4745	501	58368	11	14	13	21	21	38
08-03-15	22	61	43	59	4738	502	58281	8	9	8	17	10	19
08-03-15	23	63	46	66	4701	457	58269	7	9	15	18	9	20
08-03-15	24	40	32	36	4749	463	58279	6	6	7	11	9	9
08-04-15	1	56	57	63	4711	449	58305	7	4	4	15	15	18
08-04-15	2	24	28	22	4737	456	58331	3	2	3	6	8	7
08-04-15	3	30	44	46	4718	430	58355	2	3	2	6	12	14

08-04-15	4	30	75	40	4685	367	58386	13	10	9	7	20	9
08-04-15	5	60	101	31	4725	399	58408	6	7	8	16	29	5
08-04-15	6	25	31	31	4748	424	58418	4	8	5	6	8	8
08-04-15	7	16	28	18	4745	445	58426	3	4	2	3	7	6
08-04-15	8	14	23	30	4750	462	58438	2	2	4	2	6	6
08-04-15	9	18	29	52	4762	480	58481	6	8	6	4	8	13
08-04-15	10	22	26	17	4761	477	58450	3	3	2	7	6	4
08-04-15	11	23	18	36	4753	489	58463	4	4	3	5	4	12
08-04-15	12	32	39	37	4717	493	58474	4	4	3	10	10	12
08-04-15	13	50	34	17	4703	499	58500	5	4	3	17	8	4
08-04-15	14	40	34	43	4694	546	58501	5	5	5	10	8	12
08-04-15	15	108	28	70	4647	529	58473	9	6	9	33	7	18
08-04-15	16	102	79	159	4564	534	58480	10	13	15	29	22	50
08-04-15	17	61	25	65	4599	516	58386	11	7	11	17	6	18
08-04-15	18	53	49	42	4652	502	58390	12	9	9	11	12	10
08-04-15	19	115	43	73	4676	520	58403	18	7	12	30	11	19
08-04-15	20	42	36	61	4736	539	58366	10	9	13	11	8	14
08-04-15	21	109	101	105	4756	562	58336	12	10	12	27	26	34
08-04-15	22	205	226	126	4660	466	58285	15	15	14	51	65	29
08-04-15	23	49	101	109	4592	414	58281	7	11	7	13	28	30
08-04-15	24	122	49	37	4680	450	58220	7	6	6	41	14	11
08-05-15	1	36	36	62	4687	447	58282	4	6	5	8	10	15
08-05-15	2	34	43	22	4704	436	58313	3	5	1	10	15	8
08-05-15	3	40	28	30	4712	441	58342	2	4	2	12	8	8
08-05-15	4	23	46	39	4735	454	58352	2	4	2	8	14	11
08-05-15	5	25	23	16	4750	456	58388	2	2	1	7	6	3
08-05-15	6	28	31	28	4744	451	58400	2	3	2	8	9	10
08-05-15	7	11	13	22	4735	461	58425	1	2	1	2	4	5
08-05-15	8	7	19	8	4738	467	58435	1	1	0	2	5	2
08-05-15	9	14	15	19	4741	471	58437	2	3	2	4	5	5
08-05-15	10	14	10	10	4744	486	58441	1	2	2	4	2	2
08-05-15	11	13	15	18	4737	485	58442	3	3	1	3	3	5
08-05-15	12	28	46	30	4739	475	58454	3	3	2	8	17	9
08-05-15	13	28	72	23	4731	504	58484	8	6	3	7	21	5
08-05-15	14	60	25	21	4709	532	58480	4	2	3	16	9	4
08-05-15	15	113	18	39	4654	539	58506	10	3	5	27	3	13
08-05-15	16	97	61	109	4600	540	58473	18	8	11	25	15	34
08-05-15	17	91	75	78	4629	500	58460	20	12	18	22	20	20
08-05-15	18	101	80	62	4667	506	58403	15	13	15	26	20	10
08-05-15	19	35	56	48	4687	505	58420	11	8	8	8	14	13
08-05-15	20	52	52	92	4708	493	58445	13	10	9	10	12	20
08-05-15	21	71	131	74	4766	581	58360	11	18	9	17	35	16
08-05-15	22	170	142	85	4780	581	58293	25	19	15	45	43	17
08-05-15	23	134	95	160	4784	532	58262	27	14	25	40	26	46
08-05-15	24	194	115	68	4781	514	58255	12	5	7	64	31	21

08-06-15	1	102	45	53	4678	450	58313	6	10	4	32	14	14
08-06-15	2	50	79	69	4711	458	58340	5	6	4	16	24	20
08-06-15	3	22	19	44	4735	469	58390	8	5	6	4	4	13
08-06-15	4	11	9	10	4735	462	58413	1	1	1	2	2	2
08-06-15	5	33	22	15	4747	464	58416	3	2	1	9	5	4
08-06-15	6	55	52	12	4750	453	58412	7	4	5	18	17	2
08-06-15	7	27	35	22	4745	428	58415	2	3	1	7	9	5
08-06-15	8	88	38	29	4768	468	58436	6	6	5	26	11	8
08-06-15	9	33	41	35	4819	474	58452	11	6	6	8	9	12
08-06-15	10	35	101	194	4792	545	58563	8	14	19	8	28	64
08-06-15	11	82	51	79	4830	514	58577	10	6	10	24	14	25
08-06-15	12	29	42	66	4863	512	58523	5	6	9	7	11	21
08-06-15	13	62	57	37	4832	542	58477	7	7	5	17	20	9
08-06-15	14	30	57	23	4818	549	58456	7	8	3	6	14	6
08-06-15	15	128	67	109	4827	583	58502	15	11	18	37	17	33
08-06-15	16	105	128	192	4793	513	58678	25	17	26	25	29	62
08-06-15	17	105	54	140	4878	495	58688	23	13	19	27	15	41
08-06-15	18	145	168	67	4807	527	58607	24	19	11	42	52	20
08-06-15	19	236	206	212	4843	626	58595	52	31	45	64	56	40
08-06-15	20	103	145	166	4756	551	58574	19	19	27	27	32	43
08-06-15	21	250	281	201	4774	570	58484	35	30	24	73	93	56
08-06-15	22	269	278	146	4837	573	58462	21	20	32	87	79	40
08-06-15	23	122	87	363	4790	563	58342	15	16	32	29	22	124
08-06-15	24	180	118	249	4836	538	58300	32	25	34	50	30	70
08-07-15	1	79	75	96	4807	485	58307	9	9	13	22	18	28
08-07-15	2	55	120	73	4775	430	58383	7	8	9	14	39	20
08-07-15	3	77	98	141	4736	365	58400	21	23	20	14	20	28
08-07-15	4	150	103	182	4745	400	58379	30	29	50	39	31	43
08-07-15	5	26	45	27	4778	441	58430	7	7	8	6	11	4
08-07-15	6	87	106	123	4765	397	58484	33	16	33	21	28	31
08-07-15	7	53	31	30	4795	440	58446	6	4	5	17	8	7
08-07-15	8	119	183	364	4813	472	58518	44	56	65	19	32	98
08-07-15	9	382	233	282	4734	357	58604	111	67	55	98	67	58
08-07-15	10	75	108	37	4818	462	58507	15	13	12	22	36	8
08-07-15	11	97	99	123	4845	467	58536	11	20	17	31	21	35
08-07-15	12	57	59	28	4822	520	58478	6	4	4	13	18	6
08-07-15	13	81	97	80	4808	560	58520	14	13	6	18	28	22
08-07-15	14	102	99	112	4868	580	58613	16	11	20	29	25	35
08-07-15	15	169	208	378	4790	639	58582	23	41	38	54	68	101
08-07-15	16	154	153	382	4778	614	58792	43	64	54	34	33	104
08-07-15	17	203	110	153	4763	580	58674	25	16	15	58	30	38
08-07-15	18	51	40	178	4685	508	58474	17	12	14	14	9	44
08-07-15	19	73	38	55	4700	479	58416	17	11	11	16	9	12
08-07-15	20	59	66	43	4719	482	58402	15	21	13	14	15	9
08-07-15	21	52	53	48	4723	496	58425	11	15	11	12	11	13

08-07-15	22	65	54	42	4736	508	58419	12	8	9	16	14	9
08-07-15	23	84	91	94	4790	547	58407	11	9	9	19	27	26
08-07-15	24	101	71	72	4780	512	58371	10	6	7	35	19	18
08-08-15	1	61	52	73	4759	483	58321	7	7	7	20	17	24
08-08-15	2	59	25	74	4745	461	58349	8	5	5	13	7	19
08-08-15	3	52	27	34	4724	446	58381	9	7	3	13	7	10
08-08-15	4	42	102	47	4757	442	58390	4	6	7	12	27	15
08-08-15	5	53	33	119	4763	376	58468	8	8	9	16	8	29
08-08-15	6	190	137	112	4767	371	58513	32	28	29	49	43	26
08-08-15	7	34	42	50	4810	466	58476	4	6	4	8	9	13
08-08-15	8	21	32	15	4786	493	58455	3	5	2	5	7	3
08-08-15	9	40	41	30	4805	500	58462	6	8	5	11	14	5
08-08-15	10	92	133	237	4843	484	58580	17	16	19	32	45	78
08-08-15	11	73	102	74	4839	471	58519	11	9	6	19	30	18
08-08-15	12	84	72	89	4877	522	58555	9	9	9	22	23	19
08-08-15	13	115	45	95	4898	537	58551	16	10	6	32	12	28
08-08-15	14	61	55	94	4861	548	58503	7	10	6	21	12	24
08-08-15	15	74	84	63	4870	501	58438	10	10	7	24	27	15
08-08-15	16	124	89	152	4875	510	58497	12	11	11	32	24	51
08-08-15	17	179	109	123	4728	537	58503	36	18	13	40	26	34
08-08-15	18	122	90	212	4678	500	58490	31	14	19	33	24	54
08-08-15	19	313	169	218	4757	559	58522	66	26	47	98	56	48
08-08-15	20	324	169	309	4739	582	58420	53	28	32	86	48	93
08-08-15	21	426	288	183	4686	572	58382	46	26	28	125	90	43
08-08-15	22	171	112	104	4629	457	58384	14	18	12	50	28	29
08-08-15	23	139	101	55	4688	466	58344	14	15	10	41	24	17
08-08-15	24	73	53	67	4751	470	58368	10	10	9	23	15	20
08-09-15	1	61	19	30	4727	457	58364	5	3	3	13	5	10
08-09-15	2	40	27	24	4755	464	58385	9	4	4	10	8	5
08-09-15	3	24	45	19	4742	447	58394	10	6	3	5	14	4
08-09-15	4	39	48	41	4724	407	58408	9	7	2	10	11	11
08-09-15	5	66	38	40	4722	386	58443	8	7	8	15	8	10
08-09-15	6	88	93	41	4763	406	58463	7	7	8	24	26	11
08-09-15	7	53	54	60	4813	460	58510	12	7	15	12	15	14
08-09-15	8	35	33	70	4813	475	58529	10	10	10	8	7	18
08-09-15	9	86	123	126	4804	466	58550	20	29	26	19	26	28
08-09-15	10	72	43	38	4812	491	58491	10	7	8	21	12	10
08-09-15	11	51	48	31	4784	517	58486	6	7	4	15	11	7
08-09-15	12	99	147	196	4750	563	58632	15	9	13	29	48	56
08-09-15	13	76	53	149	4716	509	58570	10	4	10	23	18	44
08-09-15	14	55	32	47	4693	518	58477	10	7	13	14	6	12
08-09-15	15	145	106	191	4714	503	58581	27	19	26	30	29	58
08-09-15	16	118	43	72	4770	545	58525	16	6	8	33	10	21
08-09-15	17	122	99	84	4866	550	58524	13	11	16	38	25	25
08-09-15	18	149	102	79	4935	579	58479	19	7	20	40	29	24

08-09-15	19	228	75	69	4943	608	58444	28	13	19	60	19	17
08-09-15	20	234	99	138	4709	492	58364	29	13	21	54	25	32
08-09-15	21	191	170	135	4750	568	58435	30	30	22	60	51	32
08-09-15	22	346	259	184	4776	573	58334	38	31	18	117	93	51
08-09-15	23	86	66	50	4707	479	58307	15	19	14	22	13	11
08-09-15	24	145	103	126	4748	461	58336	25	27	28	34	26	23
08-10-15	1	77	50	91	4771	470	58287	7	6	11	20	12	27
08-10-15	2	36	54	53	4722	439	58356	5	9	5	9	13	16
08-10-15	3	47	26	26	4732	430	58392	12	6	5	11	7	7
08-10-15	4	23	54	52	4733	396	58414	5	12	6	4	16	16
08-10-15	5	53	46	29	4766	388	58461	6	7	6	16	13	7
08-10-15	6	56	78	258	4786	443	58523	22	14	36	14	20	79
08-10-15	7	375	342	241	4669	315	58700	79	78	59	97	95	63
08-10-15	8	19	32	118	4795	449	58537	4	5	9	4	8	37
08-10-15	9	37	49	160	4784	485	58521	7	14	15	8	11	42
08-10-15	10	141	76	155	4763	448	58603	29	16	17	31	19	42
08-10-15	11	50	45	57	4790	485	58536	8	8	11	13	9	13
08-10-15	12	40	37	29	4783	511	58508	8	6	5	9	8	6
08-10-15	13	61	18	70	4821	528	58492	6	5	5	17	5	20
08-10-15	14	80	50	14	4812	540	58456	6	3	5	27	14	3
08-10-15	15	49	37	57	4779	572	58467	8	5	4	12	10	18
08-10-15	16	102	32	56	4696	546	58507	8	5	12	28	8	18
08-10-15	17	60	49	73	4642	527	58461	17	14	12	14	13	19
08-10-15	18	136	129	139	4643	506	58478	24	18	19	33	32	44
08-10-15	19	234	86	216	4673	578	58485	20	11	14	71	20	73
08-10-15	20	94	82	83	4697	500	58398	12	11	10	25	23	22
08-10-15	21	49	73	71	4711	464	58422	21	17	16	11	18	16
08-10-15	22	65	60	41	4732	475	58415	10	17	15	18	16	9
08-10-15	23	67	124	136	4784	533	58357	11	10	14	20	34	34
08-10-15	24	61	53	112	4763	501	58360	8	5	11	17	18	29